AD- 7679

UNCLASSIFIED

AFCRC Technical Report 53-3

GEOPHYSICAL RESEARCH PAPERS

No. 18

THE DISTRIBUTION OF RADIATIONAL TEMPERATURE CHANGE IN THE NORTHERN HEMISPHERE DURING MARCH

JULIUS LONDON

December 1952

Geophysics Research Directorate

Air Force Cambridge Research Center

Air Research and Development Command

AFCRC Technical Report 53-3

GEOPHYSICAL RESEARCH PAPERS

No. 18

THE DISTRIBUTION OF RADIATIONAL TEMPERATURE CHANGE IN THE NORTHERN HEMISPHERE DURING MARCH

JULIUS LONDON

December 1952

Geophysics Research Directorate

Air Force Cambridge Research Center

Cambridge Massachusetts

ABSTRACT

The average radiation flux and flux divergence in the atmosphere during March is computed as a function of the chief absorbents of terrestrial and solar radiation, and the physical parameters of the atmosphere such as pressure, temperature and cloudiness. The infrared flux for water vapor is computed graphically from Elsasser radiation charts. The absorption of insolation by water vapor is computed with the aid of an empirical formula. The net radiation flux divergence is then computed by methods of finite differences.

It is shown that the entire troposphere constitutes an energy source insofar as radiative processes are concerned, and that at all latitudes, the largest radiational heat loss is in the middle troposphere. It is also shown that the effect of cloudiness is to concentrate this maximum radiational cooling to layers at about the height of middle cloudiness (3 to 4 km). The net heat loss at this level is found to be about 1.5 to 2.0°C day^{-1}. It is suggested that the major contribution to heating the troposphere, to offset the loss due to radiation, is the release of latent heat by condensation.

PREFACE

The major portion of this paper was originally submitted to the Graduate School of Arts and Sciences, New York University, as a doctoral thesis. The results reported represent the first completed phase of research on the heat balance project under sponsorship of the Geophysics Research Directorate of the Air Force Cambridge Research Center (Contract No. AF 19(122)-165).

It was the original purpose of the research to investigate the relationship between the latitudinal distribution of radiative excess and deficiency and various proposed models of the mean meridional circulation of the atmosphere during a transitional month (March). This purpose has since been revised to afford a more complete study of the radiative heat loss in the atmosphere. At the present time, the research is being continued along two lines. The first is to extend the present study to all seasons of the year. The second is to include other factors besides the radiative components which contribute to the atmospheric heat budget. It is hoped that the completion of this next phase of research will in part supplement our understanding of the driving mechanism of the circulations of the atmosphere.

I wish to thank Professor H. A. Panofsky, formerly of New York University and now at Pennsylvania State College, for his valuable aid and constant encouragement during all phases of the reported research, and Professor J. Spar of New York University for his painstaking review of the original manuscript.

CONTENTS

ILLUSTRATIONS

THE DISTRIBUTION OF RADIATIONAL TEMPERATURE CHANGE IN THE NORTHERN HEMISPHERE DURING MARCH*

1. INTRODUCTION

All energy of atmospheric motion is ultimately derived from incoming solar radiation. Methods for the transformation of insolational energy to that of mean motion of the atmosphere are discussed by Bjerknes et al. (1933) and Rossby (1941) among others.

Since the mean temperature of the earth and its atmosphere changes very little from year to year, incoming solar radiation must be balanced by radiation going out to space, if both radiation currents are integrated over a period of a year over both hemispheres. At any particular time and place, however, there need not be, and probably is not, a radiation balance. The transformation of energy of radiation to that of atmospheric motion is a consequence of the inequality of incoming and outgoing radiation currents as functions of time and space.

The radiation unbalance at the top of the atmosphere results from an excess of incoming over outgoing radiation in the equatorial regions, and a deficiency in the polar regions. Because of the large difference between the temperature of the sun and that of the earth and its atmosphere, the spectral distributions of the energy of solar (short-wave) and terrestrial (long-wave) radiation are almost completely mutually exclusive. As a result, the atmosphere is semitransparent to solar radiation but almost opaque to terrestrial radiation.

Only a small portion of the energy of the incoming solar beam is used directly to heat the atmosphere. The rest is either reflected back to space, or is used to heat the earth's surface and evaporate moisture from the large bodies of water. The energy which reaches the earth's surface is then transferred to the atmosphere by conduction and eddy convection in the form of sensible heat and in the form of latent heat. These constitute the major heat sources for the atmosphere.

It was shown by Möller and Mügge (1931) that the atmosphere, at least through the troposphere, continually loses heat through long-wave radiation. Since the absorption of insolation by the atmosphere is comparatively small, the atmosphere provides a heat source insofar as radiative processes are concerned. This was first clearly indicated by Möller (1935). Subsequent investigations (Elsasser (1940 a), Tanck (1940)), while limited in scope, have substantiated this fact.

The purpose of this study is to present a unified picture of the latitudinal and vertical distribution of average radiative heat loss in the northern-hemisphere troposphere. The study covers both clear skies and conditions of average cloudiness. This is to provide an estimate of the importance of cloudiness to the problem of the atmospheric radiation budget. The month of March was chosen for the research because the radiation budget of the atmosphere during March in many ways resembles the average annual budget. It is hoped that, in the future, similar studies can be made for the other months of the year, thus providing a more complete description of the role played by the atmosphere as a radiative heat source.

* Manuscript received for publication 30 July 1952.

A few words might be included at this point concerning the methods used in calculating the short-wave and long-wave radiation fluxes and the net flux divergence.

The depletion of the solar beam has been studied experimentally by Fowle (1915), Kimball (1927) and others, and theoretically by Yamamoto and Onishi (1949 a, 1951). Their results are in good agreement with those of Fowle and Kimball. The calculations of absorption of insolation by water vapor in the atmosphere are straightforward, albeit tedious.

The computations of long-wave radiation flux, however, are complicated by the fact that the infrared absorption spectrum of water vapor is extremely variable. For this reason most previous investigators such as Simpson (1928), and others have had to make simplifying assumptions concerning the absorption coefficients of water vapor which, although certainly valid for establishing the correct order of magnitude of the net outward flux at the top of the atmosphere, could not show up the correct detailed distribution of the radiation flux.

A graphical method of integration of the basic radiative transfer equations was first developed by Mügge and Möller (1932 b), thus providing for a more exact computation of the net radiation flux in the atmosphere. With increased knowledge of the water vapor absorption spectrum, came more sophisticated methods of computing radiation flux. Elsasser (1940 b) developed a new radiation chart by devising a method of expressing the extremely variable water vapor absorption coefficients by an analytic function which was both simple and accurate enough to be of practical value.

The difficulties encountered in interpreting and applying spectroscopic theory and data to water vapor absorption in the atmosphere have led to a more direct experimental approach to the problem of infrared radiation in the atmosphere. Emissivity measurements in the laboratory and the atmosphere made by F. A. Brooks (1941), Elsasser (1941), Robinson (1947, 1950) and others, indicate certain empirical relationships between emissivity and total path length of the emittent. These relationships were used by D. L. Brooks (1948) and Robinson (1950) to construct radiation charts which are quite similar to those developed by Mugge and Möller, and by Elsasser. As a matter of fact, Elsasser (1942) and D. L. Brooks have both shown the equivalence of the radiation charts constructed on the basis of spectroscopic theory and observations to those constructed by using emissivity measurements primarily. The present computations of infrared radiation flux make use of the Elsasser radiation chart, because it is felt that, despite some of the incomplete spectroscopic resolution of the infrared spectrum, it provides the more general basis for the theoretical and empirical solution to the transfer problem in the atmosphere.

There are indications, based on a study by Yamamoto and Onishi (1949b), that minor revisions to the Elsasser Radiation Chart are needed. The effect of these revisions are estimated by Yamamoto (1950). Other recent comments and criticisms of Elsasser's solutions to the transfer problem are discussed in Section 2 of this report.

The net radiative flux divergence computed in this study is derived from the smoothed vertical distribution of the radiation flux. The values of the temperature changes were then calculated from the flux divergence between discrete levels.

Methods have been suggested by Bruinenberg (1946), D. L. Brooks (1950), Hales (1950) and Cowling (1950 b) for computing point radiative temperature changes in the atmosphere from the distribution of the flux divergence. These methods, however, are of the nature of mathematical refinements, consisting essentially of devices for smoothing discrete sets of data. In the case of average flux distribution, they are probably no more accurate than the more primitive methods used in the present calculations.

2. THE THEORY OF INFRARED RADIATIVE FLUX IN THE ATMOSPHERE

2.1. THE RADIATIVE TRANSFER EQUATION

The basic equation for downward directed monochromatic radiative transfer through an absorbing slab in the atmosphere is given by the Schwarzschild equation (e.g., Brunt (1939))

$$dI_\nu = -k_\nu \sec \zeta (I_\nu - I_{b,\nu})\, du, \tag{1}$$

where I_ν is the intensity of the incoming radiation beam at the frequency ν; k_ν is the absorption coefficient per unit density per unit length of the absorbent; ζ is the zenith angle of the incoming beam; $I_{b,\nu}$ is the monochromatic black-body radiation emerging from the slab and du, the optical depth of the slab, is defined by $du = \rho dz$, where ρ is the density of the absorbent and z is height designated as positive upward.

The solution to the transfer equation for the total infrared flux was given by Elsasser (1940 b) as

$$F = \int dT \int_0^\infty \frac{df_{b,\nu}}{dT}\, \tau_f(l_\nu, u)\, d\nu \tag{2}$$

where T is the temperature, $f_{b,\nu}$ the specific black-body flux, τ_f is a function representing the transmission of radiative flux and l_ν, a generalized absorption coefficient, is the value of k_ν averaged over a small interval of the infrared spectrum.

One of the chief difficulties in evaluating Eq. (2) is that, while in theory it should be possible to determine the form of the transmission function τ_f, in practice this is no simple task.

The absorption spectra of atmospheric gases such as water vapor, carbon dioxide and ozone are, in general, band spectra where each of the absorption bands is composed of a large number of narrow absorption lines. The relationship between the absorption coefficient and the frequency for these spectral lines is of the form shown schematically in Fig. 1 (e.g., Dennison (1928)). In Fig. 1, ν_0 represents the frequency at the center of the line, and the half width α is defined as the frequency interval for which the absorption coefficient at the center of the line has been reduced to one half of its value. The total intensity of the spectral line is given by

$$S = \int_{-\infty}^{\infty} k(\nu)\, d\nu. \tag{3}$$

Ladenburg and Reiche (1913) have shown that in the case of a single absorption line (or widely spaced lines), the absorption takes place in the central portion of the line for small optical depths and is proportional to the product of the optical depth and the total line intensity. As the optical depth becomes larger, however, the absorption becomes complete at the center of the line and further absorption takes place in the line wings, where $(\nu - \nu_0) \gg 0$ and is proportional to the *square root* of the optical depth, the total line intensity and the half width of the absorption line. The fractional transmission is related to the absorption by $\tau = (1 - A)$ where A is the fractional absorption in the frequency interval $\Delta\nu$.

The above analysis has been extended by Elsasser (1938, 1942) to the case of absorption in a band spectrum where the band is composed of an infinite train of equally spaced lines, each of the same half width and total intensity. The transmission function for a beam of radiation is then given in terms of the error function of argument $\sqrt{lu/2}$, where the generalized absorption coefficient l is defined as $l = (2\pi\alpha S)/d^2$. Here α and S are the half width and total intensity of each absorption line, respectively, and d represents the distance between lines. In the case of absorption through a horizontal layer in the atmosphere, it is shown

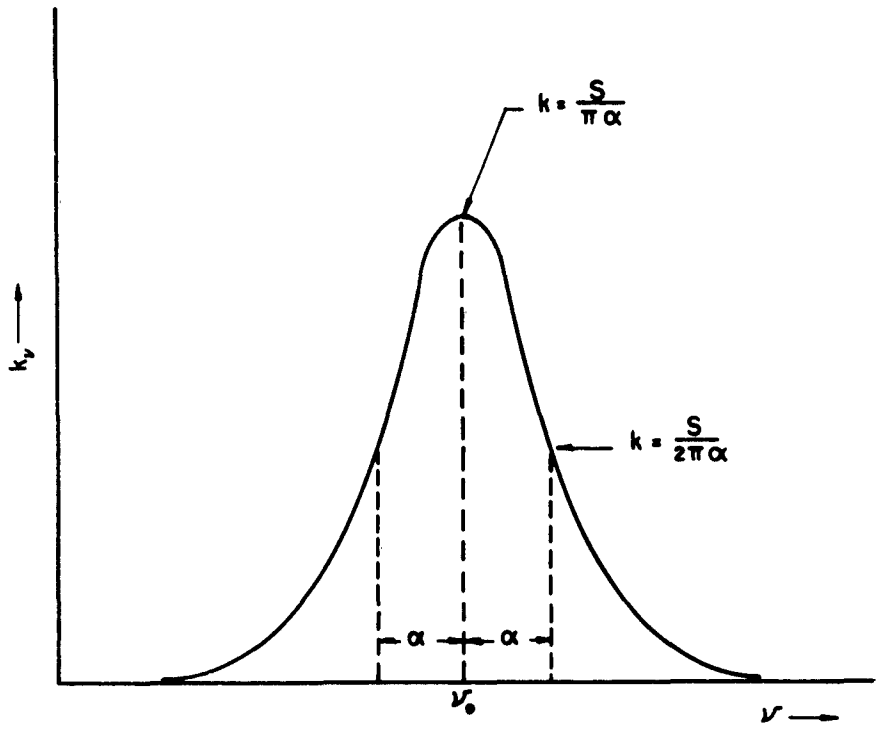

Fig. 1. Shape of a spectral line (schematic).

that the transmission function for the radiation flux becomes

$$\tau_f = [1 - \mathrm{erf}\,(\sqrt{lu/2})g\,(lu/2)], \tag{4}$$

where $g(lu/2)$ is an algebraic function which can be evaluated numerically. If Elsasser's model is reduced to a single absorption line, Eq..(4) can be reduced to the solution of Ladenburg and Reiche.

More recently, Matossi, Mayer and Rauscher (1949) have discussed the total absorption for overlapping lines of equal half widths but different total intensities and distances between the line centers. This problem is solved by an approximate method, and here again it is shown that, for a single absorption line, the approximate solution for overlapping lines reduces to the exact solution given by Ladenburg and Reiche. It is also shown that in the case of large values of the path length, the square-root law of Ladenburg and Reiche is certainly valid for overlapping lines as far as the dependence on the path length is concerned.

These results have been confirmed experimentally by Chapman (1950) using a low dispersion prism spectrometer on the water vapor bands in the near infrared. The observations indicated that the relationship between the fractional absorption in these bands and the total water vapor at constant pressure is of the form given by Elsasser. For a large range of values of the water vapor length, the relationship takes the form of the square-root absorption law.

Cowling (1950 a) has recently derived a semiempirical expression for the absorption of infrared radiation by water vapor. The expression has the form of a simple logarithmic law and it has been pointed out by Cowling (1950 b) that for calculations within the troposphere, the results are almost identical to those of Elsasser.

Finally, mention should be made of the recent extension of Elsasser's work by Kaplan (1952 a, 1952 b). Here again, the derived transmission functions give almost the same results for radiative flux computations in the lower atmosphere as those discussed above.

Since water vapor is the primary absorbent of infrared radiation in the atmosphere, the solution to the radiative transfer equation depends mainly on the determination of a general absorption law for the water vapor spectrum. The total flux can then be obtained by graphical integration as was first suggested by Mügge and Möller (1932 a), or by numerical integration as was suggested by Lonnquist (1950). A radiation chart for the calculation of the total radiation flux has also been developed by Elsasser (1940 b).

It should be noted that the development for the total flux is independent of the nature of the absorbing medium and can be applied to any absorbent in the atmosphere. Suitable transmission functions, as discussed by Craig (1949) and Yamamoto (1950), can be used in Eq. (2) for carbon dioxide and ozone, since their infrared absorption spectra are somewhat simpler than that of water vapor. At atmospheric pressures, these transmission functions would be reduced nearly to the functions for exponential absorption given by Elsasser (1942).

Although the problem of finding the exact transmission function (or functions) for the complicated infrared spectrum of water vapor has not yet been solved completely, Elsasser's results seem to be the most practical for meteorological studies of the lower atmosphere. These results, in the form of the radiation chart, have been used as the basis for most of the infrared flux calculations discussed below. The details of radiation flux computations using the Elsasser chart are discussed by Elsasser (1942) and Charney (1945).

2.2. PRESSURE AND TEMPERATURE CORRECTIONS

The expression for the total flux given in Eq. (2) was derived under the assumption that the absorption and emission in the atmosphere are independent of pressure, and dependent on temperature only through the black-body laws. Unfortunately, this is not the case.

As was shown above, for most values of optical path in the atmosphere, the total absorption in a small wavelength interval is dependent on the square root of both the optical depth and the half width of the absorption line. Although the total intensity of the absorption line is independent of pressure and temperature, the shape of the line, shown in Fig. 1, is affected by a number of factors. For our analysis, the most important of these is the broadening of the line as a result of collisions between air molecules and the molecules of the radiating gas in the atmosphere. This effect is called pressure, or collision, broadening of the spectral lines. As a result of pressure broadening, the line becomes flatter, the half width is increased and the absorption at the center or core of the line becomes diminished, although there is an increase of absorption in the line wings. For a single absorption line, it can be shown from kinetic theory that the half width is directly proportional to the pressure and inversely proportional to the square root of the temperature (e.g., Brunt 1939).

The pressure effect in the line wings is decreased for overlapping absorption lines, such as those studied by Elsasser. Thus, a smaller pressure effect should be expected. Elsasser (1942) points out that numerous investigators have shown that for a large range of the infrared spectrum, in the cases where there is a sufficient amount of the absorbent (H_2O, CO_2, or O_3), so that the square-root law of absorption holds, the total absorption varies as the fourth root of the air pressure. This would indicate that under these conditions the half width is proportional to the square root of the pressure.

This square-root pressure correction has been verified by Callendar (1941) and Elsasser (1942) for the 15-μ band of carbon dioxide based on the measurement of Hertz. On the other hand, Möller (1944) has concluded from Wimmer's observation of the 4.3-μ band of carbon dioxide that insofar as absorption is a function of optical path, the optical path for carbon dioxide should be corrected by a factor $(p/p_0)^{.73}$ where p_0 is standard sea-level pressure.

Strong and Watanabe (1940), and Summerfield and Strong (1941 a, 1941 b) have also indicated that as a result of overlapping of line wings, the pressure correction for infrared absorption of ozone and water vapor in the troposphere is of the form $A = bp^{1/4}$ where A represents the fractional absorption and b is a proportionality constant. This result is implied for carbon dioxide as well. Chapman (1950) in measuring the fractional absorption in the 1.35-μ and 1.85-μ water vapor bands, finds a similar pressure correction. The effect of pressure on the 6-μ band of water vapor has been investigated by Matossi and Rauscher (1949), who similarly find that the total absorption is very nearly proportional to the fourth root of pressure. Their results, however, are dependent on the values of the half width in the 6-μ band determined by Nielsen (1941) of 0.52 cm^{-1}. This half width is somewhat larger than that given by Adel (1947) who found that for atmospheric water vapor lines at 18.6 μ and 15.99 μ, the half width is 0.12 cm^{-1} and 0.11 cm^{-1}, respectively. Since the smaller the half width, the less is the wing effect for constant optical depth, it would seem that there is still some doubt as to the exact correction due to pressure broadening.

In the stratosphere it is most likely that, except for the rotational band of water vapor in the far infrared, the individual spectral lines become well separated from each other and, as suggested by Strong and Plass (1950), a linear pressure correction would prevail. The amount of the absorbents in the stratosphere, however, is quite small, and the difference between a linear and square-root pressure correction would be important only if one wanted to investigate the detailed flux and flux divergence distribution in the stratosphere. Since this study is confined to a model principally within the troposphere, the square-root correction is used throughout.[†]

The radiation flux as given in Eq. (2) is a function of the product $l \cdot u$. The square-root pressure correction can therefore be expressed as a correction to the optical depth. Thus for the sake of convenience, we write

$$u^* = \sqrt{\bar{p}/p_0}\, u, \tag{5}$$

where u^* is the effective optical depth, $\bar{p}$ is the average pressure in the layer considered and p_0 is standard sea-level pressure (1013 mb).

Very little is known about the relationship between line shape and temperature in the case of band spectra. The above discussion, however, leads to the conclusion that the half width of spectral lines in the infrared should be inversely proportional to the fourth root of the absolute temperature and should be included in the correction considered in Eq. (5). In the troposphere, the temperature correction would always be close to unity and it has been omitted in the calculations below.

3. THE PHYSICAL MODEL OF THE ATMOSPHERE IN THE NORTHERN HEMISPHERE DURING MARCH

It has been shown in Section 2 that the distribution of radiation flux and radiation cooling is primarily a function of the distribution of parameters characterizing the physical state of the atmosphere. The model of the atmosphere described in this section is, for the most part, based on data which represent conditions prevailing during average March in the northern hemisphere. Because of the lack of data in the Arctic,

[†] More recent evidence indicates a swing of the pendulum back to a linear pressure correction. It can be shown, however, that this would not seriously affect the calculations for the lower and middle troposphere.

the present model is limited to the region 0° to 70° N. The following discussion covers the distribution with height and latitude of atmospheric pressure and temperature, cloudiness and the chief absorbents of terrestrial and solar radiation such as water vapor, ozone and carbon dioxide.

3.1. TEMPERATURE AND PRESSURE

3.11. Troposphere

The temperature and pressure distributions used in this study were obtained from the Northern Hemisphere Upper Level Charts for March published by the U. S. Weather Bureau (1944). The data on these charts are in the form of isopleths of temperature and pressure for the entire northern hemisphere. Temperature and pressure values were averaged from these charts for each 10 degrees of latitude (0° to 70° N) around complete latitude circles, for each level of published data. From these, the vertical distributions of pressure and temperature were calculated. It was necessary to use extrapolated values for the equatorial regions since the isopleths were not generally drawn south of about 10° N. For this reason, the temperatures for the 0° to 10° N latitude belt, particularly in the upper levels, were adjusted to agree with the data published by Wagner (1931), Ratner (1946) and Hess (1948).

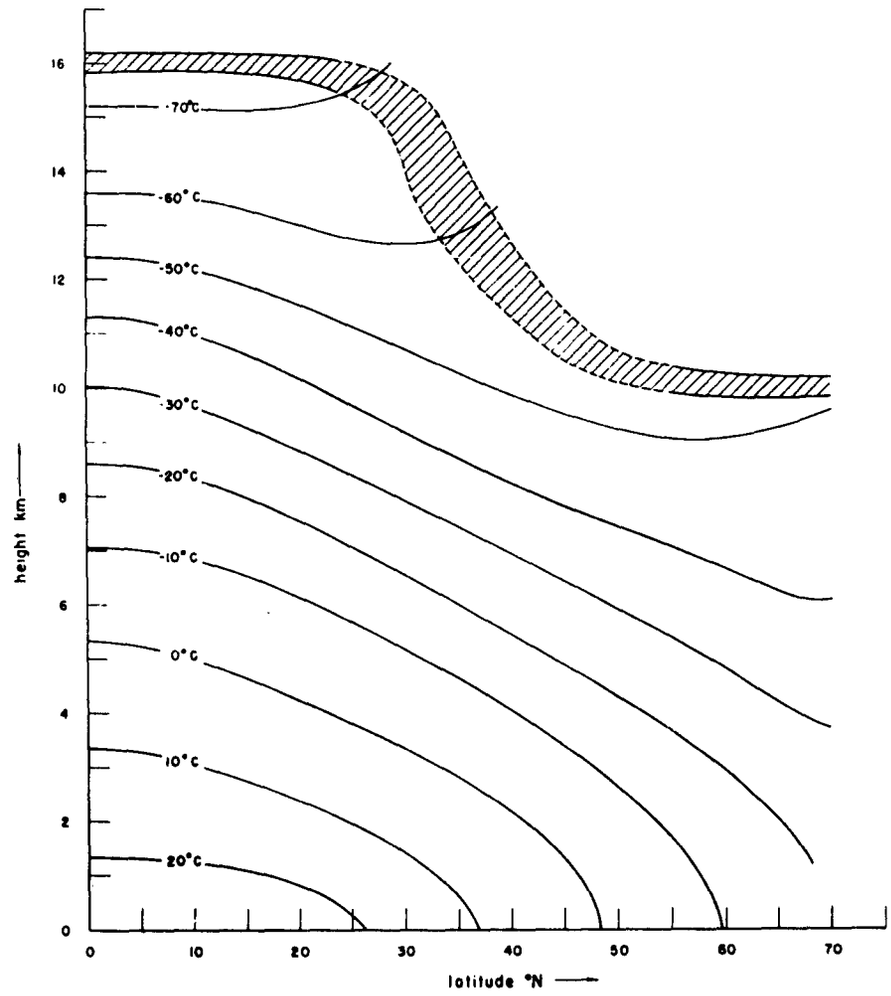

Fig. 2. Temperature distribution in the troposphere and average height of the tropopause during March (0° to 70° N).

3.12. The Height of the Tropopause

The tropopause was considered to be the upper bounding "surface" for most of the radiation flux computations. By use of the vertical distribution of temperature discussed above, it is possible to depict an approximate variation with latitude of the height of the tropopause. In the middle latitudes, the tropopause becomes indistinct and in fact is a relatively deep zone of transition rather than a discontinuity of lapse rate. The average heights used here for the middle latitudes follow from the definition of the height of the tropopause suggested by Flohn (1947). Flohn defines the "height of the tropopause" as the level at which the average lapse rate curves above and below the "tropopause layer" intersect. A vertical cross section showing the distribution of temperature and the variation of the height of the tropopause during March is shown in Fig. 2.

3.13. Stratosphere

The radiation flux downward from the stratosphere comes from a layer extending from the tropopause to a height of about 25 km (e.g., Karandikar (1946)). If we assume that the pressure distribution in the stratosphere is such that the pressure is reduced by about one half for each 5-km elevation (Penndorf (1946 b), Grimminger (1947)), that is,

$$p_h = 2^{-(h/5)} p_0,$$

where h is in km, we can easily calculate the approximate average pressure for this radiating layer. Since the tropopause slopes downward toward the poles, the average pressure of the lower stratosphere (to about 25 km) will increase with increasing latitude.

The number of calculations and observations of temperature in the lower stratosphere has steadily increased within the last five years. (For reference, see Best et al. (1947), Cox et al. (1949), Murgatroyd and Clews (1949) and Brasefield (1950), each of which contains ample references to this point.) Although these observations and calculations are not consistent in either time or place, they help to form a pattern of the thermal structure of the lower stratosphere which, for the most part, agrees well with the data presented by Penndorf (1946 a, 1946 b) and Chiplonkar (1940). During all seasons the lower stratosphere is either isothermal or has a slight inversion up to at least 25 km. The average temperature in the stratosphere between 60° and 70° N is about 25°C higher than in the equatorial belt. The radiation flux from the stratosphere is very insensitive to changes of average temperature of 5°C and/or average pressure of 10 mb. This is primarily because of the low concentrations of most of the absorbents at these high levels. (See the sections on the distribution of water vapor, ozone, and carbon dioxide.)

3.2. THE DISTRIBUTION OF CLOUDS

Clouds act as black-body radiators for infrared radiation, and varying reflectors for visible radiation. It is therefore important to know the distribution of cloudiness by cloud type as well as the average height and thickness for each type.

The most authoritative study of the distribution of total cloud cover for both northern and southern hemispheres is that conducted by Brooks (1927). This study gives the average total cloud cover over the land and over the oceans for each 10° latitude belt for each month of the year. Unfortunately, the total cloud cover has not been broken down into groups of cloud types.

For the present paper, two basic sources were used to determine the distribution of total cloud cover with latitude and the percentage of cloud cover by each cloud type. The results were then compared with those of Brooks as a qualitative check on the distribution of total cloudiness. The basic sources are:

1. Preliminary Climatic Atlas of the World (1943), which gives the total cloudiness by months in percent of total sky, for about 200 selected land stations over the northern hemisphere.

2. Atlas of Climatic Charts of the Oceans (1938), which gives the seasonal frequency of total cloud cover and of cover by various cloud types over the oceans.

The data from the Climatic Atlas of the Oceans were averaged over the winter and spring seasons to give approximate values for March. Means of the values of total cloudiness were taken for 5° squares of longitude and latitude from both atlases, and from these, the average total cloud cover for each 10° latitude belt between 0° and 70° N was computed. The following table shows the comparison between Brooks' values and those computed in the present study, of the distribution of total cloudiness, in percent, for March.

If the total cloudiness is weighted by the relative area in each 10° belt, the average cloud cover for the region 0° to 70° N is 48.2 percent according to Brooks' data and 50.0 percent according to the present study. The agreement for both the distribution of total cloudiness with latitude and the average cloudiness for the region 0° to 70° N is good, particularly in view of the fact that Brooks used data for only about one half the ocean area for the northern hemisphere. The agreement justifies the use of the data from the atlases mentioned above for the breakdown of the total cloudiness into percentage amounts of each cloud type.

Table 1. The distribution of total cloudiness in percentage of sky cover during March.

Latitude °N		Brooks	Present Study
0°–10°	Land, L	48	55
	Oceans, O	50	47
	L + O	49	49
10°–20°	L	29	32
	O	47	45
	L + O	39	41
20°–30°	L	33	34
	O	50	50
	L + O	41	44
30°–40°	L	44	46
	O	55	59
	L + O	49	54
40°–50°	L	52	53
	O	68	69
	L + O	57	60
50°–60°	L	55	54
	O	62	63
	L + O	57	56
60°–70°	L	52	53
	O	67	—
	L + O	54	53

The percentage of each cloud type was calculated from the data given in the Atlas of Climatic Charts with the aid of the same method used in determining total cloud cover. In this calculation, however, the following assumptions were made:

1. The percentage of sky covered by each cloud type is given by the percentage frequency reported for each type multiplied by the percentage of total cloud cover.

2. There is no overlap of clouds. (That is, the total cloudiness for any latitude belt is the same as the total of the observed amounts by cloud types for that belt.)

The first assumption introduces possible sources of errors for the following reasons:

1. The data used for the distribution by cloud type are for the oceanic regions only and these have been used to describe the distributions over the entire latitudinal belts. This is less serious in lower than in higher latitudes, since the ratio of ocean-to-land surface decreases with increasing latitude. The computed distribution of low cloudiness is affected more than that for middle or high cloudiness, since low clouds are more influenced by local terrain.

2. The cloud data used are based on observations at 1200 GMT. Diurnal variations of cloudiness, then, are not reflected in the averages for local observations, but rather in the cloudiness distributions about the latitude belt. Also, the difficulty of observing high clouds during the night would indicate that observations over the Pacific Ocean (where local time of the observations is near 2400) do not show the true cloudiness amounts in that region.

The second assumption (no overlap of clouds) required slight adjustments of the observed data of cloud type amounts since values for total cloudiness were computed from two sets of complementary data. This modification, however, did not change any of the amounts by more than five percent of their values and in most cases the change was much less.

For convenience, the different cloud types were put into the following six quasi-homogeneous groups: (a) cirrus, cirrocumulus, cirrostratus; (b) altostratus, altocumulus; (c) stratus, stratocumulus, fracto-cumulus; (d) nimbostratus; (e) cumulus; (f) cumulonimbus. The following table shows the average cloud amount by cloud groups for 10° latitude belts for March, with values given in percentage of cloud cover.

It is seen from the table that the Ns and St generally increase whereas the Cu and Cb generally decrease with increasing latitude.

Table 2. The distribution of average cloud amounts by groups, during March. (Values are given in percent of sky covered by each cloud group.)

Latitude °N	Ci	As	Ns	St	Cu	Cb	Total
0°–10°	12.1	5.0	6.3	7.6	13.5	4.5	49
10°–20°	10.3	4.9	4.1	6.6	11.2	4.9	41
20°–30°	10 6	6.2	4.8	8.4	10.7	3.3	44
30°–40°	12 0	7.1	7.7	14.1	10.4	2.7	54
40°–50°	10.9	7.3	10.9	18.2	9.7	3.0	60
50°–60°	9.6	6.3	11.3	16.9	9.1	2.8	56
60°–70°	7.9	6.0	11.2	17.0	8.4	2.5	53

Table 3. The distribution of average cloud heights by groups (heights are tabulated in km).

Latitude °N	Ci	As	Ns		St	Cu		Cb	
			Tops	Bases		Tops	Bases	Tops	Bases
0°–10°	9.8	4.4	4.4	1.5	1.5	2.3	1.5	5.0	1.8
10°–20°	10.4	4.8	4.8	1.8	1.8	2.8	1.8	5.7	2.3
20°–30°	10.4	5.0	5.0	2.0	2.0	3.0	2.0	6.0	2.5
30°–40°	10.0	4.7	4.7	1.8	1.8	2.8	1.8	5.4	2.3
40°–50°	8.7	4.0	4.0	1.3	1.3	2.3	1.3	4.7	2.0
50°–60°	7.6	3.6	3.6	1.2	1.2	2.2	1.2	4.3	1.7
60°–70°	7.2	3.6	3.6	1.0	1.0	2.0	1.0	4.0	1.5

Very few studies have been made of the variation of cloud height with type and latitude. Süring (1931) has given an estimate of the variation for middle and high clouds based on observations made prior to 1930. Tabular summaries are presented in Shaw's *Manual of Meteorology* (1936) and in the Hann-Süring *Lehrbuch der Meteorologie* (1938), of average summer and winter heights for 11 cloud types for some dozen stations located at latitudes ranging from 6° S to 70° N. Monthly averages of the heights of cloud bases are given in the *Airways Meteorological Atlas* published by the U. S. Weather Bureau (1941) for about 55 stations in the United States.

Means of the summer and winter values tabulated by Shaw and Hann-Süring, and the March values tabulated in the *Airways Meteorological Atlas* were plotted for each cloud group as functions of latitude. Smooth curves were then drawn to approximate these values, and the curves were used to determine the average height of the base and top of each cloud group for each 10° latitude belt (from 0° to 70° N).

It is obvious that a number of approximations must be made in order to keep the cloud data in a reasonable working form and free from unimportant and cumbersome detail. For the present study it is assumed that:

1. The various cloud types can be put into six quasi-homogeneous groups (as discussed above).
2. The tops and bases of the altostratus-altocumulus groups can be approximated by one mean height for each 10° latitude belt.
3. Nimbostratus cloud tops extend to the altostratus level.
4. Cumulus clouds have depths ranging from 3.5 km at 20° to 30° to 2.5 km at 60° to 70°.
5. Nimbostratus, stratocumulus and cumulus clouds have the same base heights in any latitude belt.

The average value of the height of each cloud group (Table 3) is a maximum for all groups at latitudes 20° to 30° N and decreases to a minimum at 60° to 70° N.

3.3 THE DISTRIBUTION OF WATER VAPOR

3.31. Troposphere

Water vapor is the chief absorbent of infrared radiation in the atmosphere. For the radiative flux calculations, therefore, it is necessary that the water vapor distribution with both height and latitude be determined with a fair degree of accuracy. Unfortunately, most observations of moisture content of the atmosphere have been for heights below 5 or 6 km. These observations would suffice for a general estimate of the

radiation flux because of the controlling nature of the physical parameters of the lower troposphere on the large-scale radiation budget. The detailed water vapor distribution throughout the troposphere is of major importance, however, in a study of radiative temperature changes because we then must evaluate the divergence of the radiation flux.

Empirical formulas giving the vertical distribution of vapor pressure with height have been discussed by Shaw (1936), Hann-Süring (1938), Brunt (1940), Yamamoto (1949) and others. These formulas, based on observations of water vapor content at low levels, are chiefly of the form

$$e_h/e_0 = f(h), \tag{6}$$

where e_h is the vapor pressure at height h, e_0 is the surface vapor pressure, and $f(h)$ is an exponential function.

During the course of the present study, 4-year averaged soundings for March for 10 different stations in the United States were analyzed in an attempt to fit the moisture data to the suggested empirical relationships discussed above. The results were not satisfactory. Further attempts were made to fit the data by the method of least squares, using the relationship suggested by Hann-Süring,

$$e_{h,\phi} = e_0\, 10^{-(ah+bh^2)}, \tag{7}$$

where the coefficients a and b were determined from the data. It was found that the coefficients did not vary systematically with latitude, and in particular, the coefficient of the quadratic term varied by as much as 2 orders of magnitude. Thus, even by varying the coefficients for each latitude, the results, particularly in the higher levels, were not sufficiently accurate for use in the radiation flux and flux divergence computations. At the tropopause, for instance, where the temperature is assumed to be known, the relative humidity derived from the least-square formula varied from 2 to 3 percent to over 300 percent for various latitudes. An analytic expression apparently cannot be used to represent accurately the vertical distribution of water vapor, particularly in the upper levels of the troposphere.

The distribution of relative humidity in the atmosphere shows a much smaller vertical variation than does that of vapor pressure or specific humidity. A more fruitful approach to the moisture distribution problem would be to assume a reasonable vertical distribution of relative humidity and from this, since the temperature distribution is known, to derive the vertical variation of water vapor directly.

The surface distribution of relative humidity, as a function of latitude, is given by Szava-Kovats (1938) for average January and July. The data represent 10-year averages of observations taken at about 6000 stations spread over the earth. Since Shands (1949) has shown that the distribution of water vapor in the lower atmosphere in March is better approximated by winter than by summer conditions, the average values of surface humidity for March were computed by weighting the January values 3 times as much as those in July. Any bias in the data because of the diurnal variation of relative humidity at the surface was eliminated by the process of averaging the data over complete latitude circles.

Average values of relative humidity for March for levels from 1 to 8 km were tabulated from the data given by Ratner (1946). At the level of the tropopause, the relative humidity was assumed to be near saturation. This assumption is supported by observational evidence published by Dobson et al. (1946), Barrett et al. (1949 a) and others. The values tabulated from Ratner's data, along with those derived for the surface and assumed for the tropopause, were plotted as functions of height for each 10° latitude belt. A 2-dimensional field of relative humidity was constructed from which it was possible to deduce the relative humidity distribution in the upper levels of the troposphere. The vertical and latitudinal distribution of

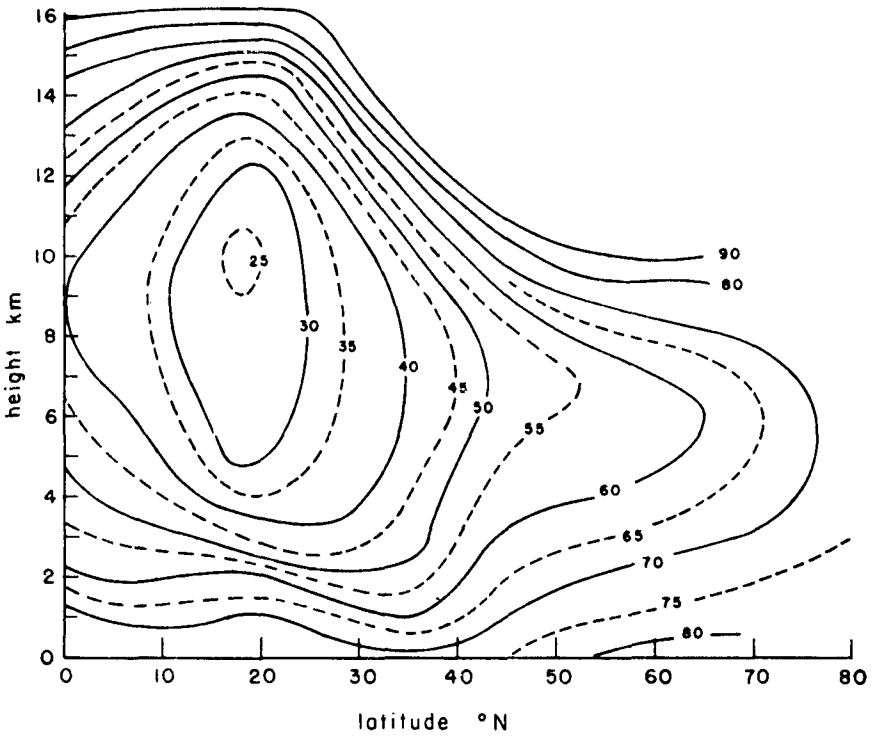

Fig. 3. Assumed distribution of relative humidity (%) in the troposphere during March.

relative humidity (Fig. 3) shows an axis of dry air at about 9 to 10 km over the equator to about 6 km at 60° to 70° N. Along this axis, the relative humidity changes from a minimum of about 25 percent at 20° N latitude to about 60 percent at 60° to 70° N.

The distribution of specific humidity (and total water vapor path length) with height and latitude through the troposphere can now be computed since the temperature, pressure and relative humidity are given. As was indicated in the preceding paragraph, since the variation of relative humidity in the atmosphere is much less than the variations of vapor pressure or specific humidity, this numerical method will give more accurate results for the moisture content distribution than would the approximation formulas discussed previously.

The total water vapor content between any two levels z_1 and z_2 in a vertical column of unit cross section is given by

$$u = \int_{z_1}^{z_2} \rho_w \, dz = (\bar{q}/g)(p_2 - p_1), \tag{8}$$

where ρ_w is the density of the water vapor in the layer, p_2 and p_1 are the pressures at the bottom and top of the layer, $\bar{q}$ is the mean specific humidity in the layer, and g is the acceleration of gravity. From Eqs. (5) and (8), the effective optical depth for water vapor is

$$u^* = (\bar{q}/g)\sqrt{\bar{p}/p_0}\,\Delta p, \tag{9}$$

where $\bar{p}$ is the average total pressure in the layer Δp, and p_0 is standard sea-level pressure.

3.32. *Stratosphere*

As a result of improved instrumentation in recent years, there have been a number of direct observations

Table 4. Summary of the distribution of average pressure, temperature and total effective water vapor content (to the tropopause) during March.

0 to 10° N				10° to 20° N				20° to 30° N				30 to 40° N			
ht(km)	*p*(mb)	*T*(°C)	u^*(gm cm^{-2})	*ht*(km)	*p*(mb)	*T*(°C)	u^*(gm cm^{-2})	*ht*(km)	*p*(mb)	*T*(°C)	u^*(gm cm^{-2})	*ht*(km)	*p*(mb)	*T*(°C)	u^*(gm cm^{-2})
0	1011	27.7	4 325	0	1013	25.3	3 381	0	1017	22 3	2.590	0	1018	13 0	1.500
1.0	900	22.8	2 575	1.0	904	20.0	1.964	1.0	896	16 5	1.377	1 0	913	9 0	0.915
1.5	856	20 6	2.070	1 8	818	15.6	1.177	2.0	792	10 3	0.716	1 8	830	5 4	0.588
1 8	826	19 2	1.775	2.0	805	14.7	1.081	2.5	747	7.7	0 528	2 0	810	4 4	0.524
2 0	802	18.2	1 560	2.3	778	13.1	0.900	3.0	703	4.7	0.388	2 3	778	2 9	0.432
2.3	780	16 9	1.378	2.8	732	10.4	0.645	4.0	622	− 1.0	0 210	2 8	727	0 2	0.305
3.0	715	13 3	0.932	3.0	712	9.3	0.553	5.0	549	− 6 7	0.108	3 0	709	− 1.0	0.267
4.0	636	7.8	0.541	4 0	631	3.5	0 282	6.0	486	−12.3	0.0528	4 0	629	− 6 3	0.149
4.4	602	5 5	0.416	4.8	572	− 1.0	0 167	7 0	427	−19.3	0 0250	4 7	578	−10.4	0.101
5.0	562	2.0	0.297	5 0	560	− 2.1	0.149	8.0	373	−26 5	0 0115	5.0	554	−12.4	0.0810
6.0	496	−3.5	0.156	5.7	511	− 6.0	0 0914	9.0	323	−33.8	0.00523	5.4	520	−15.0	0.0574
7.0	438	−10.0	0.0797	6.0	492	− 7.7	0.0742	10.0	279	−41.3	0 00249	6.0	481	−19.2	0.0372
8.0	385	−16 6	0 0391	7 0	430	−14 7	0.0349	10.4	261	−43 8	0.00182	7 0	415	−27.0	0.0163
9.0	336	−23 2	0 0181	8.0	375	−21 5	0.0162	11.0	240	−47.7	0.00124	8 0	357	−34 8	0.00738
9.8	302	−28.5	0 00967	9 0	327	−28.5	0.00740	12.0	204	−54 1	0.00061	9.0	307	−42.2	0.00361
10.0	293	−30.0	0.00797	10 0	285	−35.3	0.00342	13 0	175	−60 7	0 00034	10 0	265	−48 3	0.00198
11.0	253	−38.6	0.00312	10.4	267	−38 5	0.00236	14 0	149	−64 2	0 00019	11 0	226	−52.8	0.00103
12.0	217	−47.2	0.00121	11.0	246	−43.1	0.00151	15 0	125	−67.8	0 000073	12 0	193	−56 8	0.00045
13.0	185	−55.7	0.00049	12.0	211	−50.5	0 00067	16.0	107	−71 6	0	13 0	164	−60.0	0
14.0	156	−62.3	0.00019	13.0	181	−58.0	0.00031								
15.0	131	−69.0	0.000052	14 0	153	−63.5	0 00014								
16.0	112	−75 5	0	15 0	130	−69.0	0.000052								
				16 0	110	−74.5	0								
Stratosphere															
	65	−65.0	0.00017		65	−65.0	0.00019		62 5	−60 0	0 00028		70	−55.0	0.00164

40° to 50° N				50° to 60° N				60° to 70° N			
ht(km)	*p*(mb)	*T*(°C)	u^*(gm cm^{-2})	*ht*(km)	*p*(mb)	*T*(°C)	u^*(gm cm^{-2})	*ht*(km)	*p*(mb)	*T*(°C)	u^*(gm cm^{-2})
0	1017	4.0	1.028	0	1015	− 5.0	0.561	0	1015	−14.3	0.279
1.0	910	1.0	0.663	1.0	890	− 8.5	0.339	1.0	895	−17.0	0.181
1.3	891	0 0	0 608	1.2	870	− 9.1	0.310	1.5	835	−18.5	0.141
2.0	804	− 3 0	0.393	1 7	812	−10 8	0 234	2.0	780	−20.0	0.109
2.3	760	− 4.2	0.301	2.0	780	−11 9	0 197	3.0	677	−23.3	0.0605
3.0	698	− 7.7	0.194	2.2	762	−12 4	0.177	3.6	612	−26.7	0.0382
4.0	610	-14.0	0.0917	3.0	683	−15 3	0.104	4.0	590	−29.0	0.0326
4.7	556	−19.0	0.0538	3.6	632	−19 0	0.0699	5 0	515	−34.0	0.0190
5.0	537	−21 0	0.0442	4 0	597	−21.5	0.0522	6.0	448	−38.2	0.0114
6.0	468	−28 0	0.0205	4.3	570	−23 5	0.0411	7.0	387	−42 0	0.00678
7.0	402	−35.0	0.00905	5.0	520	−27 9	0.0257	7.2	370	−42.7	0.00570
8.0	346	−41.8	0.00422	6 0	455	−33 7	0.0133	8.0	331	−45.5	0 00353
8.7	308	−46.5	0.00237	7.0	393	−39.5	0 00659	9 0	285	−48 9	0 00146
9.0	301	−47.5	0.00211	7.6	360	−42.5	0 00433	10.0	245	−52.3	0
10.0	260	−53.7	0 00091	8.0	340	−44.5	0.00323				
11.0	222	−55.0	0	9.0	294	−49.5	0.00127				
				10.0	252	−54.3	0				
Stratosphere											
	82.5	−50 0	0.00340		84	−50.0	0 00376				

of the humidity distribution in the lower stratosphere (e.g., Glückauf (1944), (1945); Brewer et al. (1948); Barrett et al. (1950)). The data are still too few, however, to give a reliable picture of the distribution of the amount of water vapor in the lower stratosphere with latitude or season, and these observations can at best be used only as a guide to the order of magnitude of the stratospheric moisture content.

In his studies of terrestrial radiation, Simpson (1928) assumed that the stratosphere contained 0.03 gm cm^{-2} of precipitable water. On the other hand, Brunt (1940) and Sheppard (1947) have suggested that the total water vapor above the tropopause is much less, that is, something of the order of 10^{-3} to 10^{-4} gm cm^{-2}. In the absence of more complete observational evidence, it is necessary to approximate the total moisture content using reasonable assumptions based on our knowledge of the structure of the lower stratosphere.

The available observations show that the relative humidity generally increases just below the tropopause to a maximum at the tropopause and then decreases sharply, remaining less than 10 percent in the lower stratosphere. Brewer (1949) points out that this sharp decrease in relative humidity above the tropopause is probably due to the circulatior in the lower stratosphere. He suggests that air ascending into the stratosphere in the equatorial regions where it is cold and dry is transported to temperate and polar latitudes where it descends, thus accounting for a dry stratosphere at all latitudes.

To obtain an upper limit for the water vapor content of the stratosphere, it is reasonable to assume that the air is nearly saturated at the level of the tropopause, and that the specific humidity in the lower stratosphere is constant with height. Then, as suggested by Brunt and Kapur (1938), the maximum precipitable water in the stratosphere would depend only on the temperature of the tropopause.

The total mass of air above the tropopause per unit cross section is given by $M = p_t/g$, where p_t is the pressure at the tropopause. The specific humidity at the tropopause is given approximately by

$$q_t \cong 0.62(e_s/p_t),$$

where e_s is the saturation vapor pressure at the temperature at the tropopause level. Then, if we assume that the specific humidity is constant with height above the tropopause, a maximum value for the total mass of water vapor in a column of unit cross section above the tropopause (the optical depth) is

$$u = q_t \cdot M \cong 0.62(e_s/g). \tag{10}$$

The effective optical depth for the stratosphere is

$$u^* = \sqrt{\bar{p}/p_0}\, u,$$

where $\bar{p}$ is the average total pressure in the lower stratosphere. In the computations for u^*, the relative humidity at the tropopause level has been assumed as 90 percent for all latitudes. This is probably an overestimate for the polar regions, and it would have the effect of giving slightly too large downward infrared radiation in latitudes 50° to 60° and 60° to 70° N. This effect has been investigated by Hoffer (1951) and found to be quite negligible.

Table 4 given below shows, in summary form, the distribution of pressure, temperature and total effective optical depth (assuming $u^* = 0$ at the height of the tropopause) used in the present study. The data, representing average conditions for March for each 10° latitude belt (0° to 70° N), are tabulated for each kilometer up to the tropopause, as well as for the average downward radiating layer in the lower stratosphere. The heights of the bases and tops of the various cloud groups are included for convenience in calculating the radiation flux and flux divergence in the troposphere.

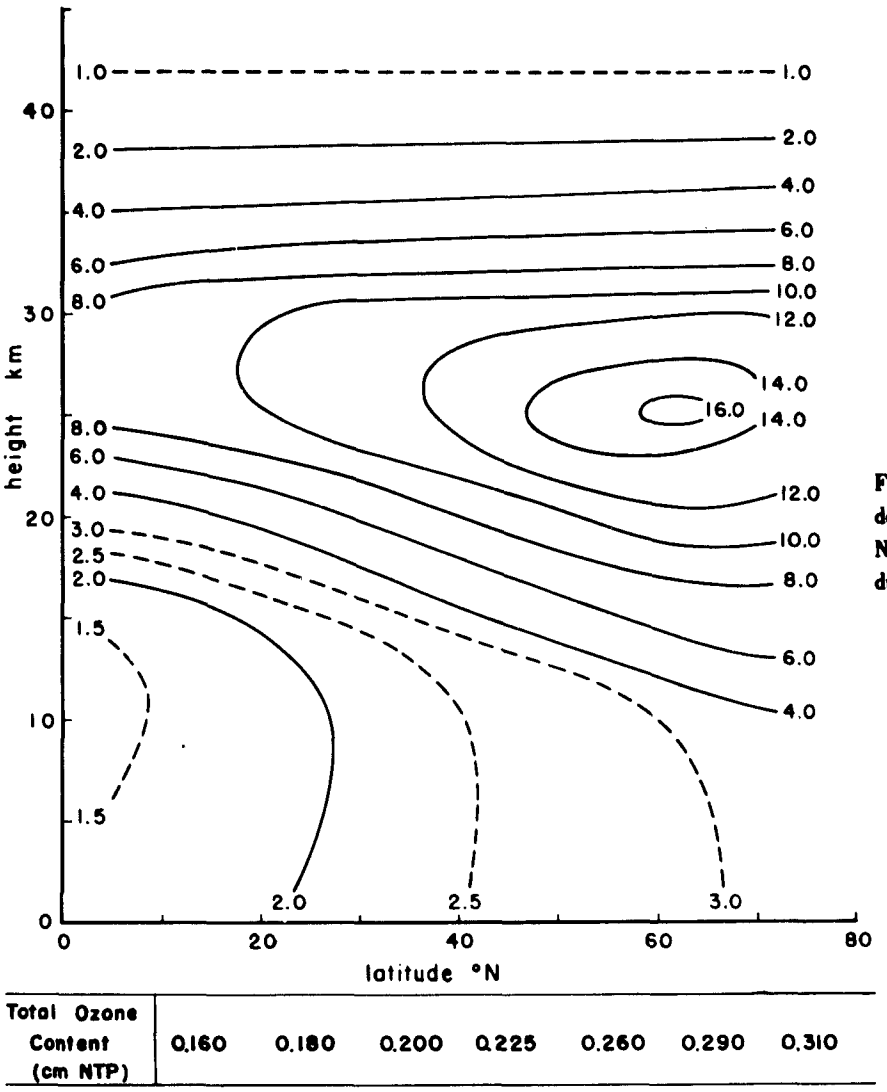

Fig. 4. Distribution of ozone density (10^{-3} cm O_3 km^{-1} NTP) in the atmosphere during March.

3.4. THE DISTRIBUTION OF ATMOSPHERIC OZONE

The ozone concentration in the atmosphere has rather large temporal and spatial variations. These variations have been discussed thoroughly by Götz, Meetham and Dobson (1934), Götz (1949) and Craig (1950). It is well established that there is a maximum amount of ozone in the northern hemisphere during March and that the total ozone content increases from about 0.25 cm (at NTP) at the equator to more than 0.30 cm in the 60° to 70° latitude (at NTP) belt, and then decreases slightly. The average values for the distribution of total ozone with latitude used in this study are taken from the study of Craig, who had the benefit of a large number of recent observations not available to the earlier investigators.

The vertical distribution of ozone has been measured and computed by means of Umkehr effect, balloon spectrograph measurements, photochemical equilibrium theory and, more recently, by rocket measurements. The data and references are all summarized by Craig. These measurements and computations show marked similarity with each other in their indicated vertical distributions, and it has been indicated by Götz (1949) that the distribution of ozone density with height is probably a function of total ozone content. The value of ozone density is uniform, and quite small from the surface layers through the troposphere. Above the tropopause, however, the ozone density increases steadily to a maximum at about 25 km, and then decreases above. Measurements made from studies in rocket spectroscopy show no significant amount of ozone above 50 km (Baum et al. (1946)). The variation shown below in Fig. 4 is based primarily on the distributions given by Götz, Meetham and Dobson (1934) and Tönsberg and Olsen (1944) with qualitative changes based on recent reports of Durant and Tousey (1947) and Regener (1950). Included in Fig. 4 are the values of the distribution of total ozone content with latitude used in the present computations.

3.5. THE DISTRIBUTION OF CARBON DIOXIDE

Observations of carbon dioxide content in the atmosphere, which have been made since at least 1867 (see Callendar (1940)), do not indicate any systematic variation in the amount of carbon dioxide either with season or latitude. The values most often quoted for the percentage volume of carbon dioxide in air varies from 0.025 (Glückauf (1944)) to 0.030 (Callendar (1940)). On the basis of observations made in England, Glückauf also has found that the carbon dioxide content of the free air is constant, at least from 4 to 10 km. Observations of the composition of the lower stratosphere (Paneth (1939)) also indicate that the percentage volume of carbon dioxide in air is constant at about 0.03 percent at least up to 30 km.

If we assume that the percentage volume of carbon dioxide to air is constant with height and latitude at 0.03 percent, we can calculate the total amount of carbon dioxide u_c in a unit vertical column from the surface to the top of the atmosphere from

$$u_c = \int_0^\infty \rho_c \, dz = (m_c/m_a) \times 3 \times 10^{-4} \int_0^\infty \rho_a \, dz, \tag{11}$$

where m_c/m_a is the ratio of the molecular weights of carbon dioxide to air, ρ_c and ρ_a are the densities of carbon dioxide and air in a unit volume of the mixed gas. Equation (11) can now be rewritten as

$$u_c = (m_c/m_a) \times \frac{3 \times 10^{-4}}{g} \int_0^{p_0} dp, \tag{12}$$

$$\sim 0.465 \text{ gm cm}^{-2}.$$

If the total carbon dioxide content is reduced to standard pressure and temperature this becomes

$$u_c' = \frac{u_c}{\rho_c'}, \tag{13}$$

where the primes indicate values at standard temperature and pressure and

$$\rho_c' = (m_c/m_a)\rho_a'. \tag{14}$$

Thus,

$$u_c' = \frac{0.465}{1.94 \times 10^{-3}} = 240 \text{ cm}. \tag{15}$$

Table 5. The vertical distribution of total effective path length for carbon dioxide in the atmosphere.

p(mb)	u_c(gm cm^{-2})	u_c'(cm NTP)	$u_c'^*$(cm NTP)
1000	0.465	240	240
900	0.418	215	204
800	0.372	192	172
700	0.326	168	141
600	0.279	144	112
500	0.232	120	85
400	0.186	96	61
300	0.140	72	39
200	0.093	48	21
100	0.046	24	8
75	0.035	18	5
50	0.023	12	3

The absorption by carbon dioxide, as in the case of water vapor, is a function of the total pressure and here again this correction can be applied to the optical path for carbon dioxide. Although the exact nature of the pressure dependency is still somewhat in doubt (see Section 2), a square-root correction has been assumed in Table 5. The vertical distribution of carbon dioxide and effective path length of carbon dioxide is given in the table.

4. CALCULATIONS OF INFRARED FLUX AND INFRARED COOLING IN THE TROPOSPHERE

4.1. COMPUTATION OF INFRARED FLUX

The infrared radiation flux computations were accomplished by means of Elsasser radiation charts (2nd ed.). For the sake of convenience, these computations were made at levels (referred to as reference levels) determined by the heights chosen as representing the tops and bases of the various cloud groups in each 10° latitude belt. This was done to avoid unnecessary duplication in the computations of the net flux in the cases of clear and average cloudy skies. The designation of these reference levels is given in Table 6.

Radiation charts were plotted for values of the total effective optical depth against the vertical distribution of temperature for each of the seven reference levels listed above for each 10° latitude belt from 0° to 70° N. The net radiation flux through each level was then determined by planimetric measurement of the areas on the Elsasser chart representing the total upward and the total downward flux through the reference level.

Table 6. Reference levels chosen for infrared flux computations.

Level	Remarks
A	ground
B	just below Stcu, base of Ns and Cu
C	tops of Cu
D	just above As, tops of Ns
E	tops of Cb
F	just above Ci
G	at the tropopause

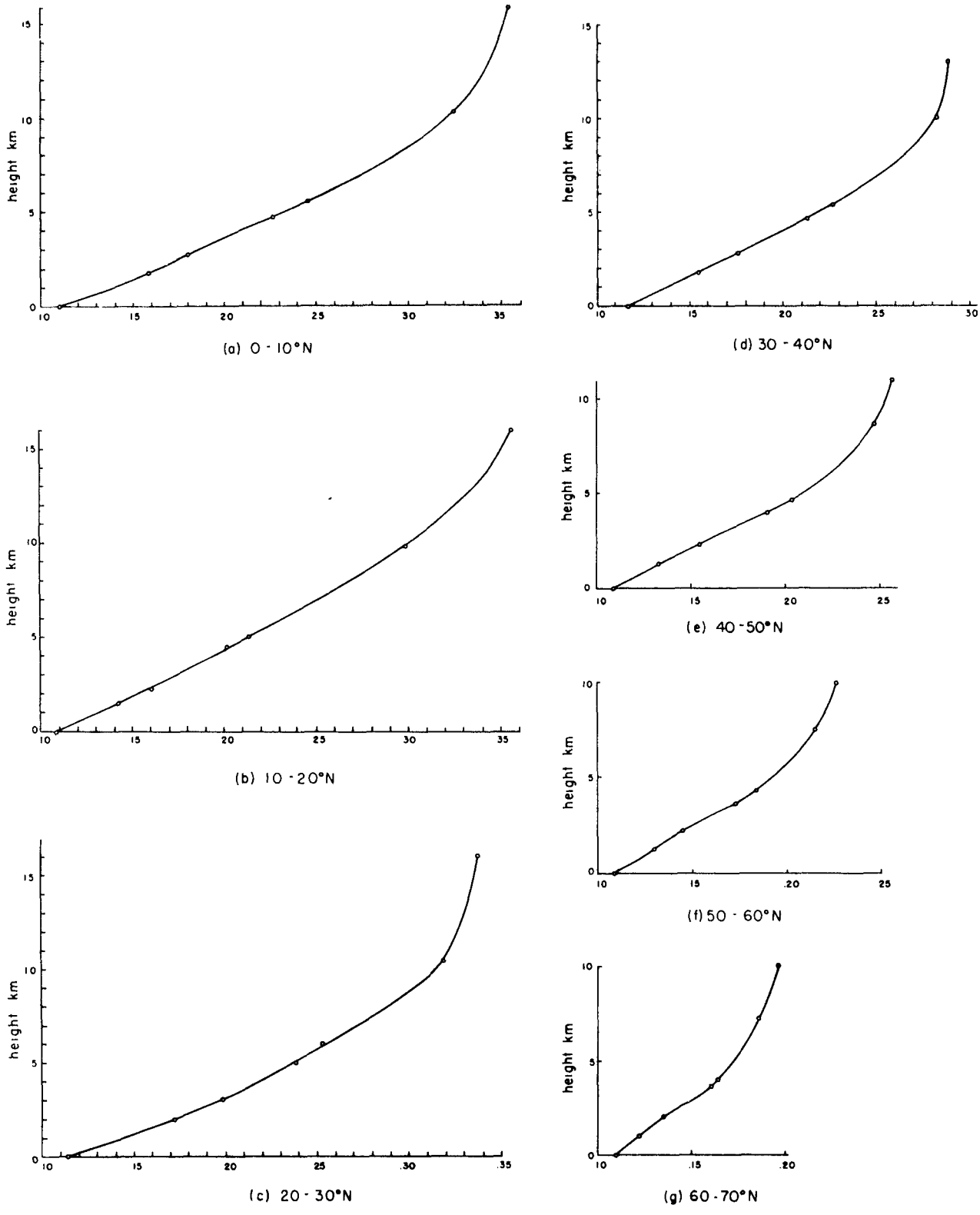

Fig. 5 (a)-(g). Vertical distribution of net infrared flux (cal cm^{-2} min^{-1}) for each 10^{o} latitude belt, *clear skies.*

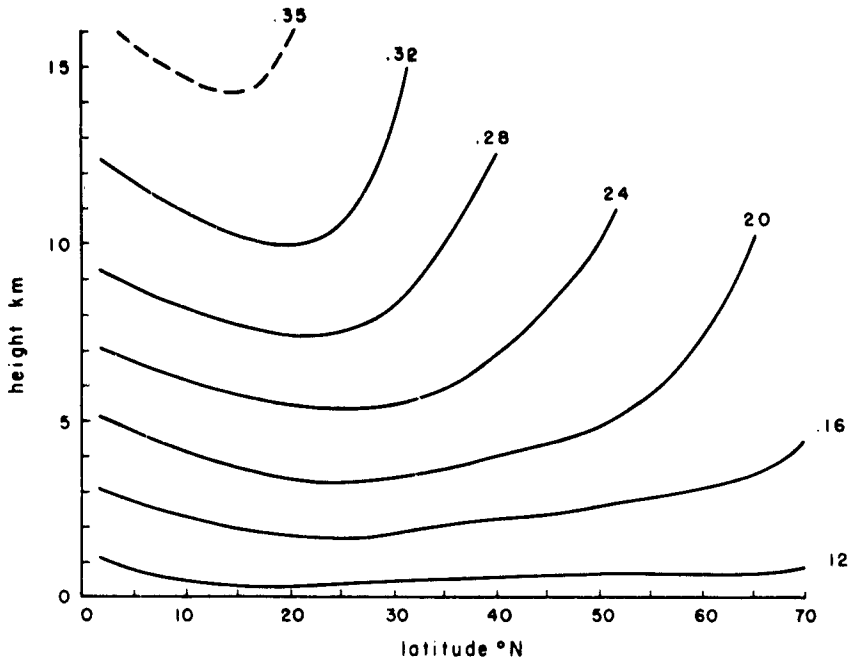

Fig. 6. Distribution of net infrared flux (cal cm^{-2} min^{-1}) in the troposphere, *clear skies.*

Table 7. The distribution of net infrared flux for March, *clear skies.*

Level	0° to 10° N		10° to 20° N		20° to 30° N		30° to 40° N		40° to 50° N		50° to 60° N		60° to 70° N	
	h	*F*	*h*	*F*	*h*	*F*	*h*	*F*	*h*	*F*	*h*	*F*	*h*	*F*
A	0	0.108	0	0.110	0	0.114	0	0.116	0	0.1095	0	0.109	0	0.110
B	1.5	0.142	1.8	0.159	2.0	0.172	1.8	0.155	1.3	0.133	1.2	0.130	1.0	0.122
C	2.3	0.160	2.8	0.180	3.0	0.198	2.8	0.176	2.3	0.154	2.2	0.145	2.0	0.135
D	4.4	0.201	4.8	0.226	5.0	0.239	4.7	0.213	4.0	0.190	3.6	0.173	3.6	0.161
E	5.0	0.213	5.7	0.245	6.0	0.253	5.4	0.227	4.7	0.203	4.3	0.184	4.0	0.164
F	9.8	0.297	10.4	0.325	10.4	0.319	10.0	0.282	8.7	0.247	7.6	0.215	7.2	0.186
G(trop.)	16.0	0.354	16.0	0.355	16.0	0.338	13.0	0.2895	11.0	0.255	10.0	0.226	10.0	0.196

h is the height of the reference level in kilometers.
F is the net infrared flux in cal cm^{-2} min^{-1}.

4.11. Clear Skies

The net flux for clear skies, calculated for seven different levels for each latitude belt, is given in Table 7. A curve of the net flux as a function of height was constructed for each latitude belt (Figs. 5 (a)–(g)) and from these curves, an atmospheric cross section (0° to 70° N) was drawn (Fig. 6) showing the distribution with height and latitude of the net infrared radiation flux for clear skies.

It is noted from Fig. 6 that the net flux is everywhere positive — that is, directed upward — and increases with height. The net flux at all levels is largely a function of the temperature at the earth's surface, since some 25 to 30 percent of the radiation flux through the tropopause comes directly from the earth's surface and this percentage is even larger for the flux through the lower levels. Other conditions being equal, the larger the water vapor content of the atmosphere, the smaller the net flux at all levels, because

there is then a larger downward flux to balance radiation from the earth's surface. Aloft, an increased percentage of the flux comes from the moist layer which is higher and, therefore, colder than the surface of the earth. Thus, the combination of high surface temperature and low atmospheric humidity results in a maximum of radiation flux at about 15° to 25° N. The low water vapor content is overbalanced by the very low surface temperatures to give minimum flux values in the more northerly regions (50° to 70° N).

At the earth's surface, with clear skies, the average net flux in units of cal cm^{-2} min^{-1} is about 0.110 with a slight maximum of 0.116 at 30° to 40° N. At a height of 10 km this net flux increases from about 0.300 at the equator to about 0.320, then decreases to about 0.195 at higher latitudes. Since the tropopause becomes lower with increasing latitude, the net upward flux through the tropopause is highest in equatorial regions (0.350 at 16 km) and lowest in polar regions (about 0.200 at 10 km).

4.12. Modifications Due to Cloudiness

In the computations described above, we have considered the net infrared flux in the atmosphere for conditions of clear skies. The presence of clouds in varying amounts and at varied heights will, of course, alter this distribution of net flux, since cloud decks radiate and absorb as black bodies in the infrared region. Computations for clear skies must then be modified by the inclusion of the black-body radiation upward at the temperature at the tops of the cloud groups, and black-body radiation downward at the temperature at the bases of these cloud groups. If one is now to compute the net flux through any level aloft, the total upward directed flux from the surface must be modified by absorption and reradiation (at temperatures lower than at the earth's surface) by the cloud groups below the level considered. Also, the downward flux is increased due to the presence of black-body surfaces (cloud decks) above the reference level which will absorb infrared sky radiation from above and reradiate this energy downward through the reference level.

The total sky is only partially covered by each cloud group. The black-body radiation from a cloud surface through any level in the atmosphere is therefore decreased by an amount indicated by the percentage of sky covered by that cloud surface. Hence, a cloud group covering only 20 percent of the sky would radiate one fifth of the black-body radiation of a sky completely overcast by that cloud group. The effect of cloudiness is to reduce the net flux at the earth's surface and at any level in the atmosphere.

Calculations of net flux were made using the same temperature-total moisture distributions as above, but now taking into account the average cloudiness for each latitude belt. The results of these calculations

Table 8. The distribution of net infrared flux for March, *average cloudiness.*

Level	0° to 10° N		10° to 20° N		20° to 30° N		30° to 40° N		40° to 50° N		50° to 60° N		60° to 70° N	
	h	*F*	*h*	*F*	*h*	*F*	*h*	*F*	*h*	*F*	*h*	*F*	*h*	*F*
A	0	0 075	0	0.084	0	0 088	0	0 076	0	0 060	0	0.063	0	0.062
B	1 5	0.096	1 8	0 117	2.0	0 125	1.8	0.098	1.3	0.073	1.2	0.071	1.0	0 066
C	2 3	0 127	2 8	0 146	3 0	0 163	2.8	0.139	2.3	0.116	2.2	0 110	2.0	0.103
D	4 4	0 172	4.8	0 199	5.0	0 210	4 7	0.185	4 0	0.168	3.6	0 151	3.6	0.143
E	5 0	0 195	5 7	0.224	6 0	0 230	5.4	0.203	4 7	0 185	4.3	0.165	4 0	0.150
F	9 8	0 271	10 4	0.296	10.4	0 282	10 0	0.249	8 7	0.222	7 6	0.197	7 2	0 173
G(trop.)	16 0	0.325	16 0	0 324	16 0	0 304	13 0	0.256	11 0	0.226	10 0	0 207	10 0	0 184

h is the height of the reference level in kilometers.
F is the net infrared flux in cal cm^{-2} min^{-1}.

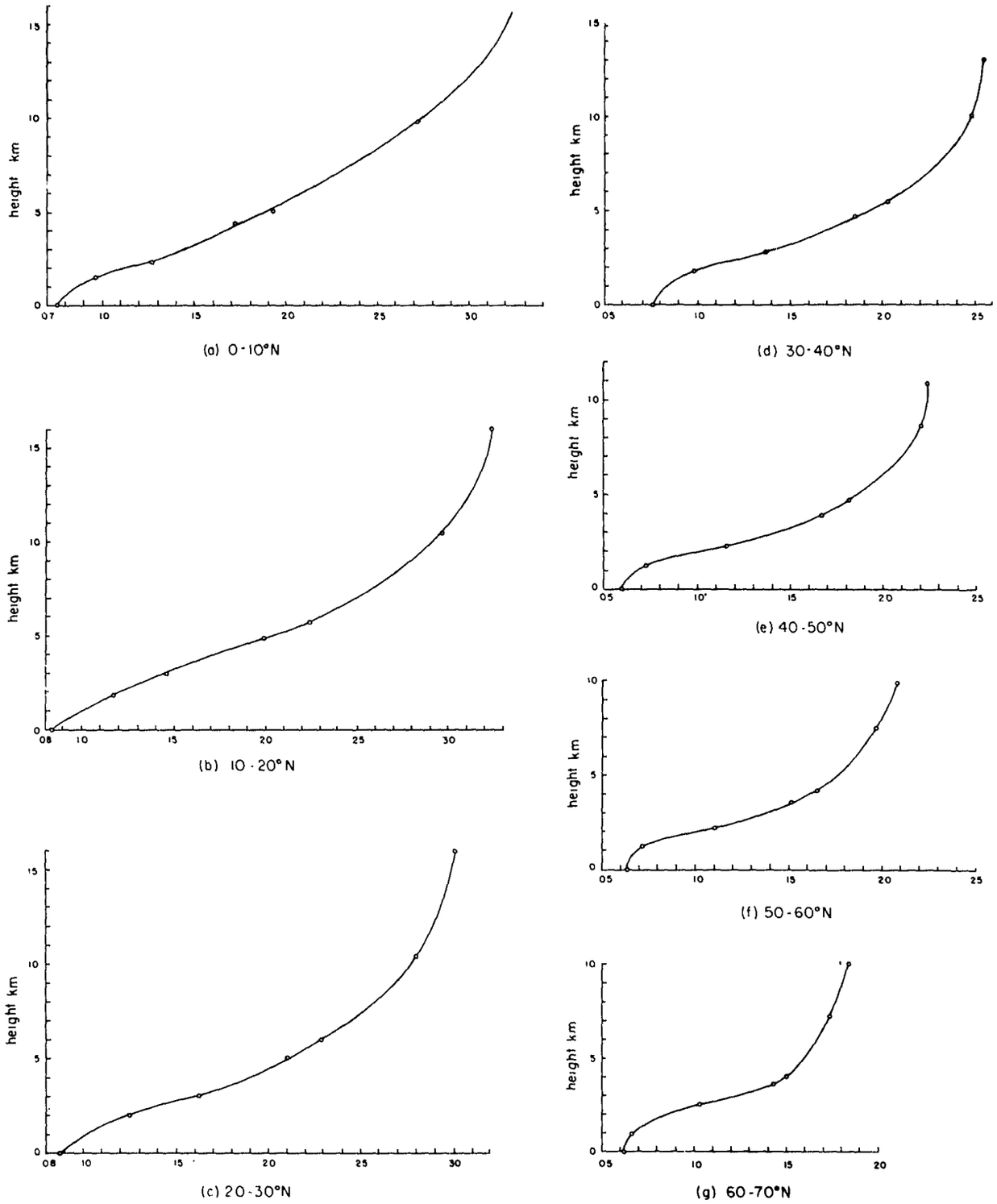

Fig. 7 (a)-(g). Vertical distribution of net infrared flux (cal cm^{-2} min^{-1}) for each 10^{o} latitude belt, *average cloudiness*.

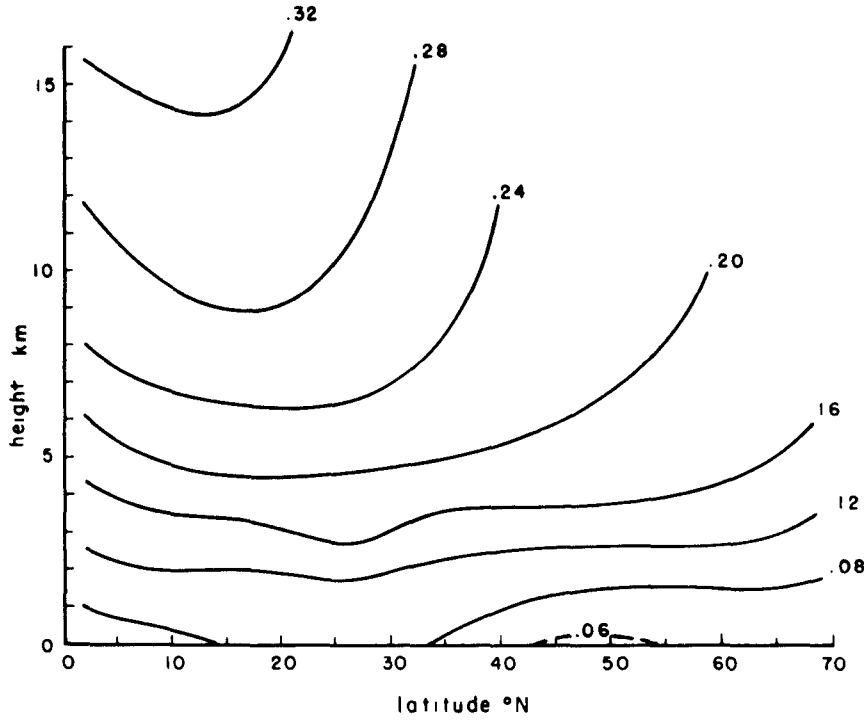

Fig. 8. Distribution of net infrared flux (cal cm^{-2} min^{-1}) in the troposphere, *average cloudiness*.

are given in Table 8. A curve of the net flux against height was drawn for each latitude belt (Figs. 7 (a)–(g)), and from these curves, values were obtained showing the distribution of net infrared flux (with average cloudiness) as a function of height and latitude. This distribution is shown in Fig. 8.

On the whole, the flux distributions for clear and cloudy skies are quite similar. The net flux for average cloudy skies is everywhere positive, increases with height, and the maximum flux at each level is again at about 20° to 25° N. Although the net flux is reduced at all levels, the difference in the net flux between the ground and the tropopause is increased for all latitude belts (in proportion to the cloudiness for that latitude belt). For instance, it is found that the net flux at the height of the tropopause is reduced by about 0.020 to 0.030 cal cm^{-2} min^{-1} or about 5 to 10 percent of its value. At the ground, the net flux is reduced by about 0.030 to 0.050 cal cm^{-2} min^{-1} or about 25 to 45 percent of its value. Thus, the presence of clouds inhibits the upward flux of radiation more from the ground than from levels aloft.

The effectiveness of cloudiness in reducing the net upward flux can also be noted when comparing Figs. 6 and 8 according to latitude. It is seen that at the ground, the smallest reduction is found at latitudes 10° to 30° N where, not only is the total average cloudiness a minimum (41 to 44 percent compared with 55 to 60 percent at latitudes 40° to 60° N) but, more important, the amount of low clouds (stratus, stratocumulus and nimbostratus) is much less than at the higher latitudes (22 to 24 percent compared with 35 to 38 percent in the more northerly regions). The effect of the heights of the various cloud groups is also clearly seen by comparing the difference of the net flux through the tropopause with clear skies against that where average cloudiness is considered. Here the reduction due to cloudiness is at a minimum in the more northerly

latitudes where, despite the larger amount of total cloudiness, the average clouds are at a lower level and therefore radiate upward at a higher temperature relative to the surface than in the case of the cloud groups at higher levels in the region 10° to 30° N.

Another very significant difference between the two distributions is the fact that, for clear skies, each graph of infrared flux against height (Figs. 5 (a)–(g)) has a positive and *almost constant* slope up to about 5 to 8 km, then an increasing slope to the height of the tropopause. In the case of average cloudiness, however, the analogous graphs (Figs. 7 (a)–(g)) have positive but decreasing slopes, *becoming almost horizontal* for heights just above the level of the middle clouds, with increasing slopes to the height of the tropopause. This difference in slopes is directly related to the difference in the distribution of infrared cooling for clear skies and for average cloudy skies.

4.2. INFRARED FLUX DIVERGENCE

It has long been recognized that for both clear and cloudy skies, the earth's surface and its troposphere continually loses heat by means of infrared radiation (Mügge and Möller 1932 a, Elsasser 1940 a). The heat loss results from the fact that most of the radiation leaving the earth's surface is absorbed by the water vapor and clouds above and then re-emitted both upward and downward at temperatures lower than at the ground. Since the amounts of both water vapor and cloudiness decrease with height, the *net* flux for a normal troposphere (temperature decreasing with height) is directed upward and increases with height for all latitudes. Strong and Plass (1950) have recently presented the view that the major contribution to radiational cooling in the atmosphere is due to the phenomenon of pressure broadening. If one considers completely separated absorption lines, a certain amount of radiation from the line wings will be continually lost to space since the pressure and therefore the half width of these lines decreases with height. This wing effect will increase the upward radiation flux as higher altitudes are reached and more and more energy, originating from lines at lower elevations, penetrates through the atmosphere without being absorbed. It is not very likely that this effect would be of paramount importance in the troposphere, since, as was indicated in Section 2, the infrared absorption bands of both water vapor and carbon dioxide are composed of numerous, partially overlapping lines. It was indicated that for overlapping absorption lines, wing radiation is probably reduced by square root rather than by linear-pressure dependence. Thus the major contribution to the flux divergence in the troposphere must come from the rapid decrease of the absorbents themselves. In the stratosphere, where most of the absorption lines become well separated, the linear-pressure correction should become valid and the effect of pressure broadening could partially explain the infrared cooling above the tropopause. Further study of the effect of pressure broadening on line width and absorption is needed to solve this problem.

To calculate the rate of radiational cooling one must be able to determine the vertical divergence of the net flux. If the radiation flux is known at all levels, the infrared radiational temperature change per unit time, in a unit volume, can be computed from the first law of thermodynamics,

$$dF_n = -c_p \frac{T}{\theta}\frac{d\theta}{dt}\rho\, dz, \tag{16}$$

where c_p is the specific heat of air at constant pressure and θ represents potential temperature. If we neglect the effect of advection and compression, the right side of Eq. (16) defines an effective temperature change given by

$$dF_n = -c_p \frac{\partial T}{\partial t}\rho\, dz. \tag{17}$$

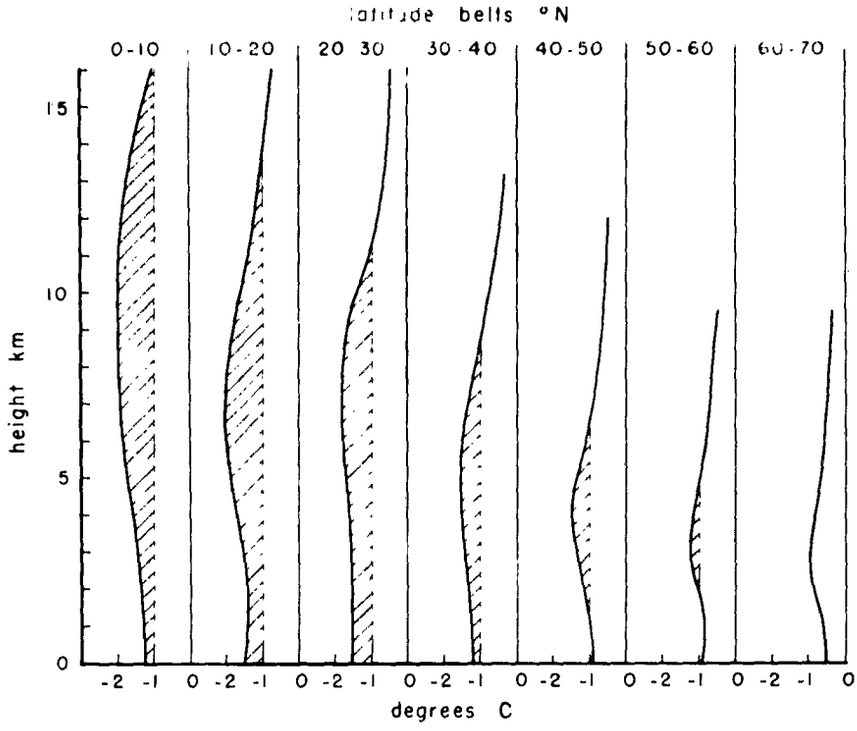

Fig. 9. Vertical variation of average infrared cooling (°C day^{-1}) for each 10° latitude belt, *clear skies.*

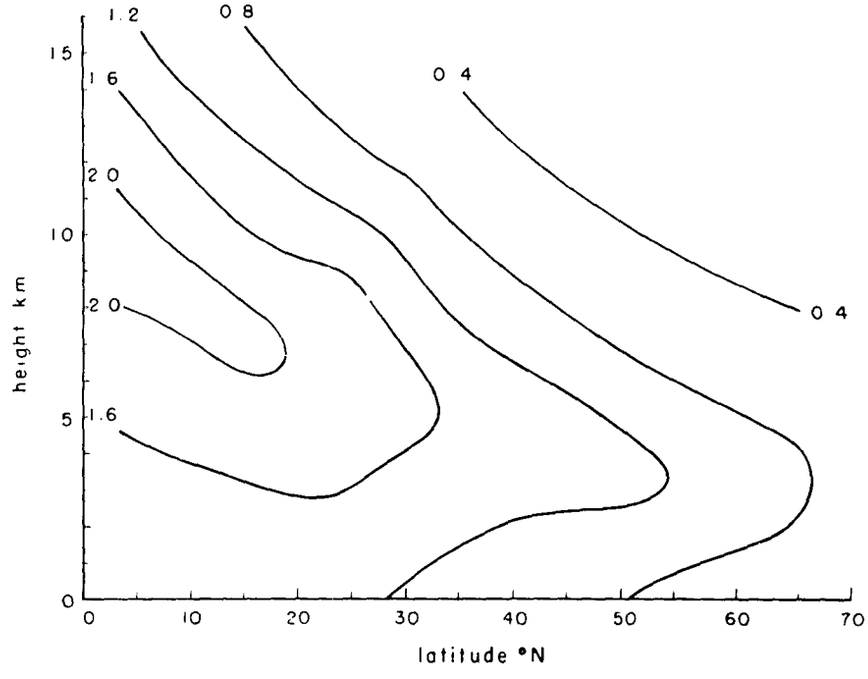

Fig. 10. Distribution of average infrared cooling (°C day^{-1}) in the troposphere, *clear skies.*

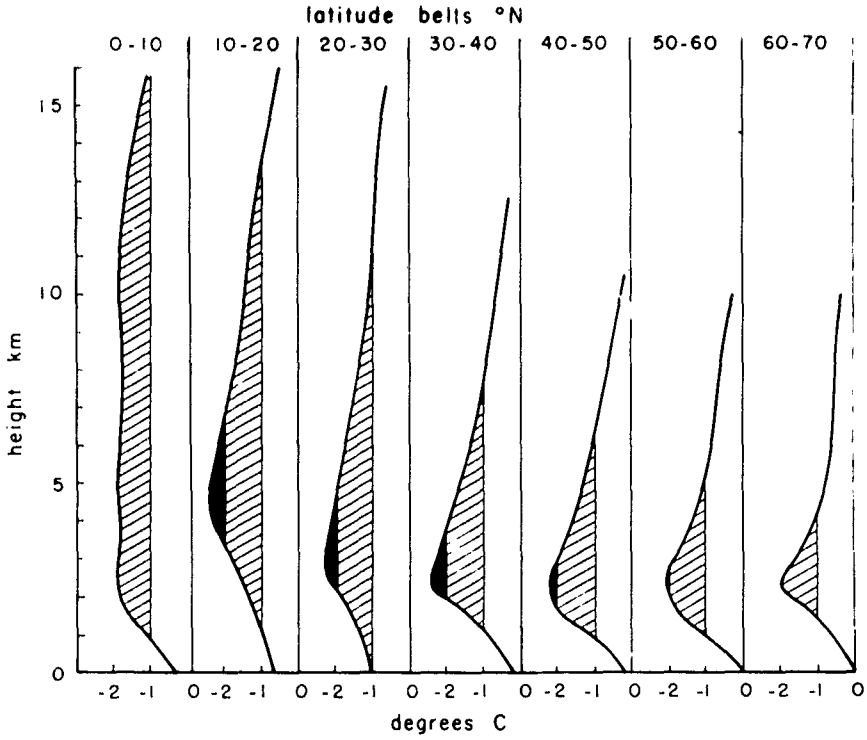

Fig. 11. Vertical variation of average infrared cooling (°C day^{-1}) for each 10° latitude belt, *average cloudiness.*

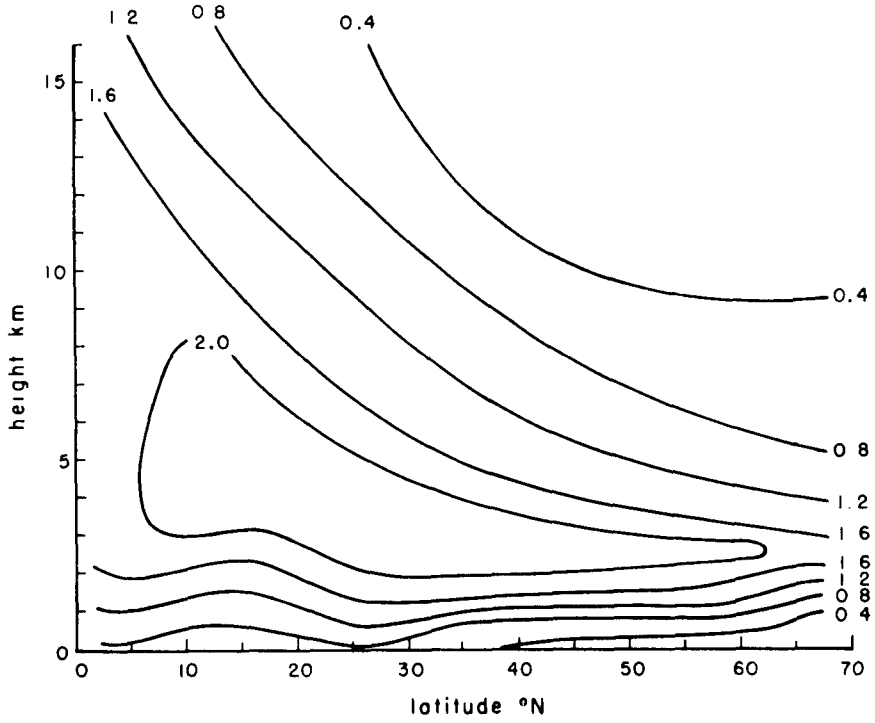

Fig. 12. Distribution of average infrared cooling (°C day^{-1}) in the troposphere, *average cloudiness.*

day^{-1}) in equatorial regions and at about 3 km (1.0°C day^{-1}) at 60° to 70° N. Thus, even in the case of clear skies, the largest infrared cooling occurs in the middle troposphere rather than near the surface of the earth. This is essentially due to the logarithmic character of the decrease of water vapor with height, particularly above the turbulence layer.

As a result of the high surface temperature and very low relative humidity aloft in the subtropical region, the layer near the earth's surface loses heat more rapidly in the 20° to 30° latitude belt than at any other latitude, with the heat loss in the surface layer being a minimum in the polar regions. Because of the high temperatures in the equatorial regions, and the consequent high specific humidities, the largest rate of infrared cooling aloft, level for level, is at latitudes 0° to 20° N. Here, the maximum of 2.0°C day^{-1} is the highest average radiative heat loss in the atmosphere.

The calculations for heights near the tropopause can only be approximate because of our inadequate knowledge of the water vapor content at these levels. The computed results give an indicated rate of cooling of 0.5° to 1.0°C day^{-1} near the tropopause. These values are in good agreement with the results of the calculations of Junge (1937) of the magnitude of the infrared cooling due to water vapor in the lower stratosphere.

4.22. Modifications Due to Average Cloudiness

The cooling distribution discussed above is changed somewhat if the average cloudiness for each latitude belt is included in the calculations for infrared radiational cooling. The overall cooling of the troposphere remains at about 1.6°C day^{-1} in the equatorial region (0° to 20° N). In the polar region (50° to 70° N), however, as a result of the predominance of low over middle or high cloudiness, the net upward flux in the lower layers is reduced, and the overall cooling rate is increased from about 0.75°C day^{-1} for clear skies to about 1.0°C day^{-1} for conditions of average cloudiness.

It is shown in Figs. 11 and 12 that at all latitudes the rate of infrared cooling increases with height from the earth's surface to about 3 to 5 km where there is a pronounced maximum and then decreases to the tropopause. By comparing the diagrams for clear and cloudy skies, one sees that clouds merely act as more effective shields for outgoing radiation than does water vapor. Cloudiness does not qualitatively change the distribution of infrared cooling.

At all latitudes near the earth's surface, the rate of cooling has been decreased as a result of the presence of low clouds. The decrease in cooling in the lowest layer is about 50 percent except in the subtropics, where the amount of low clouds is at a minimum. Here the cooling has been decreased by about 30 percent. An additional effect of cloudiness on the cooling distribution is to define more sharply the level of maximum cooling in the middle troposphere. This level of maximum cooling varies with the average height of the middle clouds and thus is at a higher elevation in the tropical than in the polar regions. The maximum of infrared cooling in the troposphere has been increased to about 2.5°C day^{-1} and is found at latitudes 10° to 30° N at about 4 to 5 km. The average cloudiness distribution does not influence the infrared flux divergence in the upper troposphere. This is indicated by the fact that the rate of cooling near the tropopause remains essentially the same (0.5° to 1.0°C day^{-1}).

The heat lost by the atmosphere through long-wave radiation is made up in part by the absorption of insolation by water vapor and clouds. This absorption is relatively small, however, as will be shown in Section 5, and the patterns of infrared cooling presented above dominate the distribution of net radiational temperature changes in the atmosphere.

4.3. INFRARED COOLING DUE TO OZONE AND CARBON DIOXIDE

In addition to water vapor, ozone and carbon dioxide also have absorption bands in the infrared region. Of the three known infrared absorption bands of ozone, only the band centered at 9.6 μ might be of meteorological significance, since it is the strongest of the three. At terrestrial temperatures, the maximum black-body radiation is centered at about 10 to 12 μ, and it is precisely in this region in the infrared that the water vapor absorption is weakest. One might suspect, therefore, that there is a significant amount of cooling due to the divergence of infrared flux due to ozone. This is found to be the case for the stratosphere (30 km). (See, e.g., Craig (1949).) In the troposphere, however, the amount of ozone present is extremely small, as shown above, and both the infrared flux and the divergence of the infrared flux due to ozone is negligible compared with that of water vapor.

Carbon dioxide has two intense absorption bands in the infrared, one between 12.5 μ and 17.5 μ and the other centered at about 4.3 μ. The former is the more important for atmospheric radiation, because it is both wider and closer to the maximum black-body radiation at terrestrial temperatures. It has been shown by Callendar (1941) that for the amounts of carbon dioxide present in the troposphere, the net flux of infrared radiation in the 12.5- to 17.5-μ band is very small. Bruinenberg (1946) and Brooks (1948) have calculated the cooling due to the flux divergence in the carbon dioxide bands and have found that this cooling in the lower and middle troposphere is of the order of one tenth that of water vapor. It has also been suggested by Deacon (1950) that for layers thicker than 100 meters the cooling due to carbon dioxide is much smaller than that due to water vapor. For very thin layers near the ground, however, the cooling could be as large.

By the use of the emissivity path length relationship for carbon dioxide given by Elsasser (1942), it is possible to compute directly the net flux due to carbon dioxide radiation at each level in the troposphere. This was done for the temperature-pressure distribution of Table 4 and the carbon dioxide distribution of Table 5. The net flux in the lower layers is positive but very small, and increases very slowly with height. Through the troposphere, the average cooling due to carbon dioxide is of the order of 0.1°C day^{-1}.

In the upper troposphere and in the stratosphere, however, the total amount of carbon dioxide is small (see Table 5) and the pressure correction to the optical path for carbon dioxide becomes important. The cooling in the stratosphere due to carbon dioxide is even larger than that due to ozone as has been shown by Oder (1948), Craig (1949) and Strong and Plass (1950).

The infrared cooling, due to ozone and carbon dioxide, has been omitted in the calculations of net radiation temperature changes in the troposphere. In view of the foregoing discussions, it is seen that this omission affects only those calculations for levels near the tropopause.

5. CALCULATION OF THE ABSORPTION OF INSOLATION AND THE RESULTING HEATING IN THE TROPOSPHERE

5.1. THE DISTRIBUTION OF INSOLATION AT THE TOP OF THE ATMOSPHERE

The incoming solar radiation received by a horizontal surface of unit area per unit time at the top of the atmosphere is given by

$$I_0 = (J/r^2) \cos \zeta, \tag{20}$$

Table 9. The distribution of average insolation at the top of the atmosphere during March.
(Unit: cal cm^{-2} min^{-1})

ϕ	0° to 10° N	10° to 20° N	20° to 30° N	30° to 40° N	40° to 50° N	50° to 60° N	60° to 70° N
I_0	0.6169	0.5928	0.5508	0.4923	0.4189	0.3330	0.2376

where ζ is the zenith angle of the sun, r is the distance from the earth to the sun in astronomical units ($r = 1.0$ when the earth is at mean distance from the sun) and J is the average solar constant determined for $r = 1.0$. The value of the average solar constant is 1.94 cal cm^{-2} min^{-1} according to Abbot (1942).

It can be shown from spherical trigonometric relationships (Humphreys (1940)) that the average insolation during any day is given by

$$I_0 = \frac{J}{r^2\pi}(\sin\phi \sin\delta\cdot\omega_0 + \cos\phi\cos\delta\sin\omega_0), \tag{21}$$

where ϕ is the latitude, δ is the declination of the sun and ω_0 is the sun's hour angle at sunrise (or sunset), given by

$$\cos\omega_0 = -\tan\phi\tan\delta. \tag{22}$$

The average insolation for each day during March was calculated for each latitude belt by use of Eqs. (21) and (22). Values of r^2 and δ for each day are given in the *American Ephemeris*. The average of the values of r^2 and δ for the four years 1920, 1925, 1930 and 1935 was used to eliminate the inequalities of δ and r on the same date in different years caused by the fact that a year does not contain an integer number of days.

In calculating the average values of I_0 for March, the arithmetic mean was taken of the daily average values during the month. The average values of I_0 were computed at latitudes 5°, 15° . . . 65° to approximate the means for the 10° latitude belts 0° to 70° N and are shown in Table 9.

5.2. THE TOTAL ABSORPTION OF SOLAR ENERGY BY MOLECULAR OXYGEN

The solar beam which enters the top of the atmosphere is only slightly depleted before reaching the ozonosphere. This depletion is to a large extent due to the absorption characteristics of molecular oxygen.

Penndorf (1950) has given an estimate of the vertical distribution of the energy absorbed per unit volume per unit time under the assumptions that:

1. absorption by molecular oxygen takes place in the wavelength region 0.11 to 0.22 μ,
2. insolation in this wavelength interval is at an effective black-body temperature of 5300°K,
3. zenith distance is 0°, and
4. the rate constant of the 3-body collision producing molecular oxygen in the E-layer is $k_1 = 1.3 \times 10^{-32}\, t/T_0$ cm^6 sec^{-1}.

The total energy absorbed per unit volume per unit time is given by

$$dQ/dv\,dt = hc\int_{\lambda_1}^{\lambda_2} A_\lambda \lambda^{-1}\, d\lambda$$

where λ_1 and λ_2 are the wavelength limits of the integration, A_λ is the number of quanta absorbed per cm^3,

h is Planck's constant and c is the speed of light. Penndorf's results show absorption of 10^{-13} cal cm^{-3} sec^{-1} at about 90 km increasing to a maximum at 102 km of about 1.5×10^{-12} cal cm^{-3} sec^{-1} and then decreasing to about 10^{-15} cal cm^{-3} sec^{-1} at about 125 km.

Results of spectrograph measurements made during rocket ascents have shown that at heights of 50 km, there is still complete absorption below about 0.23 μ. If we assume constant absorption from 50 to 90 km, the total absorption in a unit column of air per unit time would be

$$dQ/dt \simeq \int_{50}^{125} (dQ/dv\,dt) \cdot dz$$

$$\simeq 10^{-4} \text{ cal cm}^{-2} \text{ min}^{-1}.$$

The assumptions made above, upon which this value is based, would give the probable maximum absorption by molecular oxygen. This value is smaller than the total ozone absorption by a factor of *200*.

5.3. THE ABSORPTION OF INSOLATION BY ATMOSPHERIC OZONE

It has already been indicated that the direct solar beam remains almost completely undiminished until it reaches the top of the ozone layer. Through the ozonosphere, however, most of the energy in the ultraviolet region of the solar spectrum, as well as in a small portion of the visible part of the spectrum, is absorbed. The energy absorbed by ozone in the atmosphere depends on the distribution of energy in the solar spectrum, the absorption coefficients of ozone, and the total amount and vertical distribution of the ozone in a column traversed by the solar beam.

The energy distribution of the solar spectrum is very nearly that of a black-body radiator at an effective temperature of about 6000°K. Measurements by Abbot et al. (1923) and Pettit (1932, 1940), among others, gave indications that below 0.4 μ the solar energy curve drops sharply from that corresponding to a black body at 6000°K. These results have been confirmed by more recent observations taken during rocket flights at White Sands, New Mexico. The rocket measurements indicate that the insolation at the top of the atmosphere ranges from about 80 percent at 0.4 μ to about 40 percent at 0.3 μ, and to about 10 to 15 percent at 0.25 μ, of that of a black-body radiator at 6000°K (e.g., Hulbert (1947), Newell (1950)).

Ozone has absorption bands in the ultraviolet, visible and infrared regions of the spectrum. The most important bands for the depletion of insolation are the Hartley (0.22 to 0.32 μ), the Huggins (0.32 to 0.36 μ) and the Chappuis (0.44 to 0.76 μ) bands. The absorption coefficients in these regions have been the subject of many extensive investigations, the most important of which were those conducted by Colange (1927), Ny and Choong (1932, 1933) and Vassey (1941) whose results seem to be the most consistent and reliable. Craig (1950) has recently presented an excellent summary of the extant data concerning the absorption coefficients of ozone in these three bands. The data show very intense absorption in the Hartley band, with an absorption coefficient at the band center (about 0.25 μ) of about 6×10^2 cm^{-1} O_3 at NTP, decreasing absorption in the Huggins band with an average absorption coefficient of about 10^{-1} cm^{-1} O_3 at NTP, then increasing again through the Chappuis band to a maximum at about 0.59 μ of slightly larger than 10^{-1} cm^{-1} O_3 at NTP. The absorption bands for ozone in the infrared region are centered at 4.75 μ, 9.6 μ and 14.1 μ. They contribute very little to the depletion of incoming radiation, since the insolational energy in the infrared region is very small.

The monochromatic depletion of insolation by ozone in a horizontal layer of vertical depth dz is given by

$$dI_\lambda = I_\lambda k_\lambda \, n \cdot m \, dz, \tag{23}$$

where I_λ is the monochromatic intensity of a parallel beam at the top of the layer, k_λ is the absorption coefficient of ozone at wavelength λ, n is the ozone density at height z and m is the relative length of the path through which the solar beam passes and depends on the zenith angle. If Eq. (23) is integrated from height z to the top of the atmosphere, we get

$$I_\lambda = I_{0,\lambda} \exp(-\int_z^\infty k_\lambda \, n \cdot m \, dz). \tag{24}$$

Upon substitution of Eq. (24) into Eq. (23) we get an expression for the energy absorbed per unit volume along the solar beam. The energy absorbed in a wavelength interval $d\lambda$ is then

$$\frac{dI_\lambda}{m \, dz} d\lambda = I_{0,\lambda} k_\lambda n \exp(-k_\lambda \, mN) d\lambda, \tag{25}$$

where

$$N = \int_z^\infty n(z) \, dz.$$

The distribution of n as a function of height and latitude during March has been given in Section 2.

Since the integration of Eq. (25) need be carried out only over the regions of significant ozone absorption (i.e., where $I_{0\lambda} \, k_\lambda$ is not negligible) it is important to consider only the absorption in the Hartley, Huggins and Chappuis bands. For fixed values of N and m, Eq. (25) can be integrated numerically. Craig (1949) has presented the results of such an integration in the form of a graph of absorption per unit volume per unit ozone density against total path length of ozone. For the relative path length m, Craig used sec ζ. This is certainly valid for $\zeta \leq 75°$. For $\zeta > 75°$ the absorption is small since I_0 is small, and at $\zeta = 90°$ the absorption is zero because $I_0 = 0$.

The total optical path and, therefore, the absorption by ozone, changes considerably during the day. The average absorption is given by

$$\bar{a}_z = 1/2\omega_0 \int_0^{\omega_0} a_{z,\omega} \, d\omega, \tag{26}$$

where ω is the hour angle ($\omega = \omega_0$ at sunrise or sunset), $a_{z,\omega}$ is the absorption per unit volume at hour angle ω and height z. For constant ω there is little variation in N sec ζ from day to day. Thus, values of N sec ζ for March 16 were used to represent the average ozone path length during March. Values of absorption per unit volume per unit ozone density for each hour from sunrise to noon were obtained as a function of N sec ζ from the chart prepared by Craig (1949). The integral in Eq. (26) was then approximated by use of Weddle's rule where $\omega_0 \approx \pi/2$. Thus the average absorption during the day is,

$$\bar{a}_z \approx 1/40[a_{z,0} + 5a_{z,1} + a_{z,2} + 6a_{z,3} + a_{z,4} + 5a_{z,5} + a_{z,6}] \tag{27}$$

where the subscript $a_{z,i}$ ($i = 1 \ldots 6$) refers to the absorption per unit volume at height z and hour angle $i\pi/12$.

The distribution of absorption per unit volume by atmospheric ozone is shown in Fig. 13. The absorption is rather large in the upper ozonosphere (40 to 50 km) where the principal absorption is in the Hartley

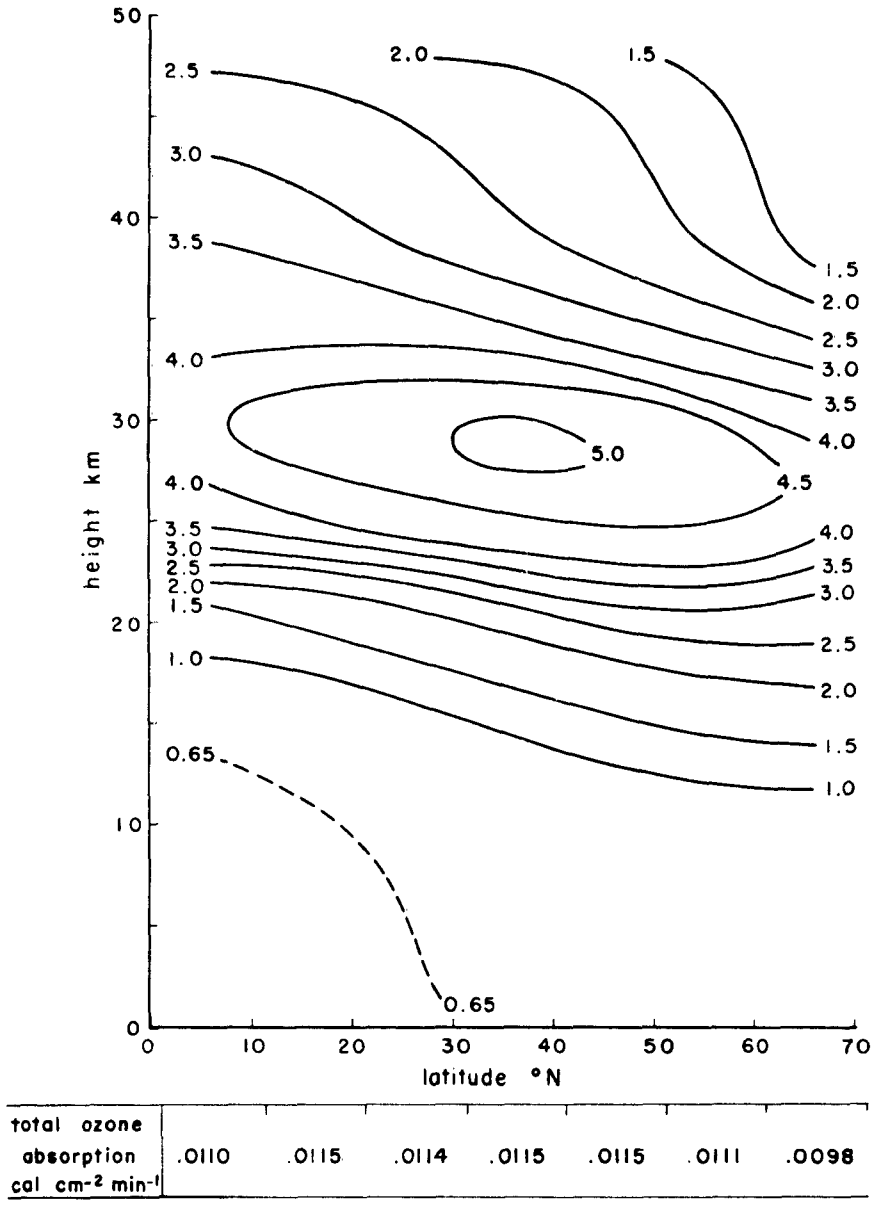

Fig. 13. Distribution of absorption of insolation (10^{-4} cal cm^{-2} min^{-1} km^{-1}) by atmospheric ozone.

band and increases to a maximum of about 5×10^{-4} cal cm^{-2} min^{-1} km^{-1} at about 25 to 30 km where the remaining insolation in the Hartley band is completely absorbed. Below about 15 to 20 km (through the troposphere), the absorption is relatively small, being about 0.75×10^{-4} cal cm^{-2} min^{-1} km^{-1}, and is due almost entirely to absorption in the weaker Huggins and Chappuis bands. The total absorption per unit area increases rapidly through the ozonosphere and is practically constant in the troposphere at a value of about 0.01 cal cm^{-2} min^{-1}. This total absorption is almost unchanged with latitude from 0° to 70° N, resulting from the fact that the insolation on a unit horizontal surface decreases while the total ozone content increases with increasing latitude. North of 70°, it appears that the total absorption should decrease rapidly, since both the total ozone content and the vertical component of insolation decrease.

The value of 0.01 cal cm^{-2} min^{-1} represents about 1.6 percent of the incoming radiation at 0° to 10° N, increasing to about 4 percent of the insolation at 60° to 70° N. The average absorption in the atmosphere due to ozone is about 2.1 percent of the average insolation for the northern hemisphere during *March*. This value of percentual absorption is lower than that given by Dobson (1942) of 5 to 8 percent and equal to that given by Fritz (1949) of 2.1 percent for the mean absorption by ozone for the year. The higher value is based on the assumption of a 6000°K black-body solar energy curve. It has already been pointed out, however, that the ultraviolet insolation received at the top of the atmosphere is only about 40 percent of that of a black-body radiator at 6000°K.

The absorption per unit volume in the troposphere by atmospheric ozone is exceedingly small. The contribution to heating in the troposphere due to this absorption is about 0.02°C day^{-1} near the tropopause decreasing to about 0.004°C day^{-1} near the earth's surface. This represents a minor component of heating in the troposphere and is neglected in the present calculations of net radiational temperature changes.

5.4. THE ABSORPTION BY WATER VAPOR

The absorption of insolation by water vapor is almost completely confined to the visible and near infrared regions since about 99 percent of the energy of the solar spectrum is contained in wavelengths below 4 μ. This absorption has been studied experimentally by Fowle (1915, 1917) and Hettner (1918), among others. Fowle determined the fractional absorption of light from a Nernst glower as a function of water vapor path length. The light was sent through a long tube containing known concentrations of water vapor at room temperature and atmospheric pressure and the absorption in each water vapor band was determined spectroscopically. The total absorption of insolation as a function of total water vapor was then calculated by correcting for the difference between the strength of the light source and the average solar constant of 1.94 cal cm^{-2} min^{-1}. Hettner's measurements, on the other hand, were carried out for water vapor at a temperature of 400°K and are not directly applicable to meteorological studies. The results given by Hettner for absorption values in the near infrared are much larger than are found for atmospheric water vapor (see Yamamoto and Onishi (1949 a)).

The absorption of insolation by water vapor in the atmosphere has been determined directly by Kimball (1927, 1930) and Hoelper (1937, 1943). These studies, based on solar radiation measurements, give the distribution of absorption as a function of total precipitable water in the path of the solar beam. The distribution of water vapor was found from various empirical formulas. A table, summarizing the results of Fowle, Kimball, and Hoelper, is given by Hoelper (1943) where a comparison of the various results shows that Fowle's corrected values for absorption of insolation are, for all water vapor path lengths, about 10 to 25 percent higher than the values given by Kimball and Hoelper, the latter two sets of values being in good agreement with each other.

Formulas for the absorption per unit volume at any height with any zenith distance of the sun were obtained by Yamamoto and Onishi (1951) using the theoretical values of the water vapor absorption coefficients obtained by them. Their results (which include a pressure correction) agree with those of Kimball and Hoelper.

Inherent in the observations used by Kimball and Hoelper was the effect of pressure broadening on the near infrared water vapor absorption bands. If the total precipitable water in the atmosphere is replaced

by the effective water vapor path length, taking into account a square-root pressure correction, Fowle's results are reduced to the average of the values given by Kimball and Hoelper.

Mügge and Möller (1932) have shown that Fowle's values can be fitted, to a fair degree of accuracy, by the empirical formula

$$a = 0.172(u)^{0.3}, \tag{28}$$

where a represents the energy absorbed in cal cm^{-2} min^{-1} in a column parallel to the solar beam containing u gm cm^{-2} of precipitable water. If u is measured in a vertical column, and we replace u by u^* (the effective optical depth for water vapor) the absorption along the solar beam becomes

$$a = 0.172(u^* \sec \zeta)^{0.3}, \tag{29}$$

where, as in previous discussions,

$$u^* = \sqrt{\bar{p}/p_0}\, u.$$

The average of the values given by Kimball and by Hoelper can be expressed by a relationship analogous to Eq. (29). That is,

$$a = 0.147(u \sec \zeta)^{0.25}, \tag{30}$$

the difference being that no pressure correction is used in Eq. (30) for the water vapor distribution. The two expressions for the water vapor absorption given above give almost the same values for a wide range of water vapor path lengths. For convenience, since the square-root pressure correction was used in the determination of total precipitable water as given in Section 3, the approximation given in Eq. (29) was used in the present calculations.

The depletion of insolation by water vapor in a vertical column extending from height z to the top of the atmosphere is then given by

$$a_{z,\zeta} = 0.172[u^*(z) \sec \zeta]^{0.3} \cos \zeta. \tag{31}$$

For the average absorption during the day, we can write an analogous expression to that used in the case of absorption by ozone. That is,

$$\bar{a}_z = 1/2\omega_0 \int_0^{\omega_0} a_{z,\zeta}\, d\omega, \tag{32}$$

where the integral in Eq. (32) is again computed numerically by the use of Weddle's rule.

As was the case for ozone for constant ω, $a_{z,\zeta}$ varies very little from day to day. To avoid a great number of tedious computations, $\bar{a}_z$ as calculated for March 16 was used to represent average values during March. Values of $\bar{a}_z$ were computed from Eqs. (31) and (32) for each 10° latitude belt (0° to 70° N) for each kilometer of height in the troposphere. The vertical distribution of absorption during March for each latitude belt is given in Table 10. The absorption by water vapor in a unit vertical column extending from the surface to the top of the atmosphere amounts to about 0.093 cal cm^{-2} min^{-1} at 0° to 10° N decreasing to about 0.021 cal cm^{-2} min^{-1} at 60° to 70° N. This represents an absorption of about 15 percent of the insolational energy received at the top of the atmosphere in equatorial regions decreasing to about 9 percent of that received in the region 60° to 70° N.

The distribution of absorption is shown by a series of curves in Fig. 14. These curves are drawn for each 10° latitude belt from the surface to 10 km. The variation of absorption with height can be represented with good accuracy by a relationship of the form $a = a_0 \exp(-bz)$ where the coefficient b varies from about

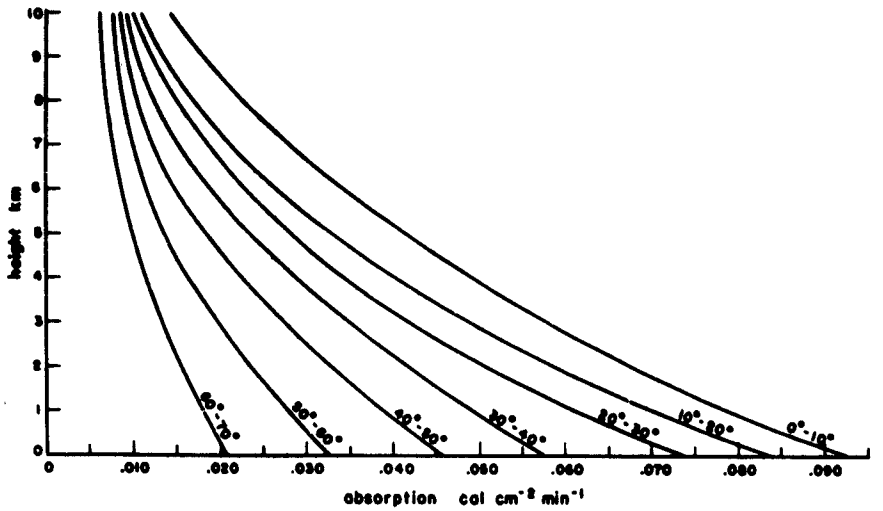

Fig. 14. Vertical variation of absorption of insolation by water vapor for each 10° latitude belt, *clear skies.*

Table 10. The average absorption of insolation by atmospheric water vapor during March. (Unit: cal cm^{-2} min^{-1})

h(km)	0° to 10° N	10° to 20° N	20° to 30° N	30° to 40° N	40° to 50° N	50° to 60° N	60° to 70° N
0	0.0929	0.0839	0.0735	0.0577	0.0458	0.0324	0.0206
1	0.0796	0.0713	0.0608	0.0496	0.0402	0.0279	0.0182
2	0.0684	0.0596	0.0500	0.0421	0.0344	0.0238	0.0157
3	0.0586	0.0487	0.0416	0.0344	0.0279	0.0198	0.0133
4	0.0498	0.0398	0.0346	0.0289	0.0224	0.0162	0.0112
5	0.0416	0.0329	0.0283	0.0242	0.0182	0.0134	0.0098
6	0.0344	0.0267	0.0229	0.0193	0.0148	0.0113	0.0087
7	0.0281	0.0213	0.0183	0.0152	0.0122	0.0096	0.0079
8	0.0227	0.0169	0.0146	0.0124	0.0105	0.0087	0.0071
9	0.0180	0.0134	0.0116	0.0106	0.0095	0.0079	0.0065
10	0.0141	0.0107	0.0094	0.0094	0.0088	0.0072	0.0060
11	0.0108	0.0086	0.0079	0.0086	0.0082		
12	0.0083	0.0070	0.0067	0.0080			
13	0.0064	0.0060	0.0060	0.0074			
14	0.0055	0.0053	0.0056				
15	0.0048	0.0048	0.0051				
16	0.0044	0.0044	0.0047				

0.16 at low latitudes to about 0.13 in the more northerly regions. This form of the absorption curves follows from the essentially logarithmic character of the effective water vapor distribution (see Section 3).

5.5. HEATING DUE TO WATER VAPOR ABSORPTION

The average heating in a thin layer due to the absorption of insolation by water vapor can be found by computing the absorption in the layer *du*. Tanck (1940) has given a formula, based on the empirical expression of Mügge and Möller, for the direct computation of average heating during a solar day resulting from absorption of insolation by atmospheric water vapor. The average temperature change in units of °C min^{-1} was given as

$$\frac{dT}{dt} = \frac{.0521}{(u)^{0.7}} \frac{\bar{q}}{c_p} Z, \tag{33}$$

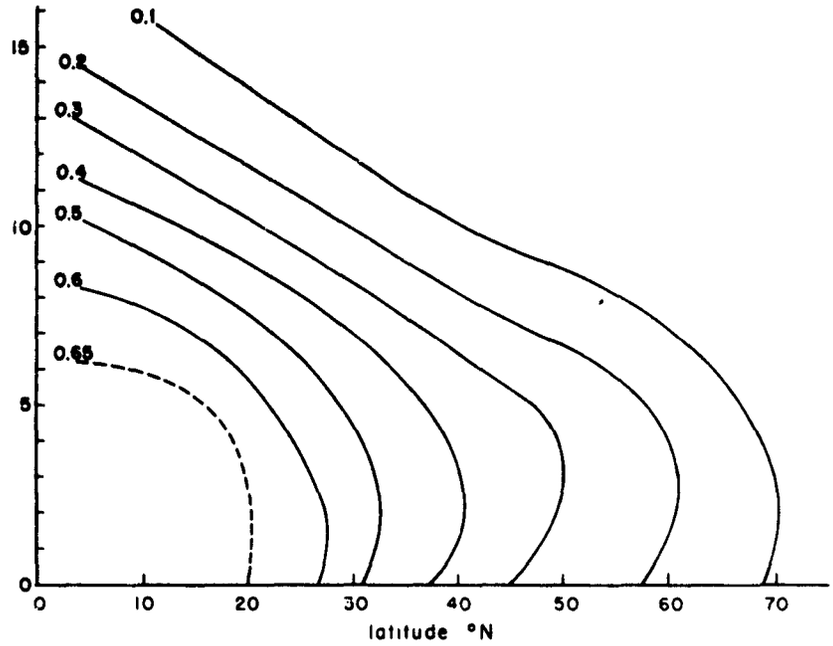

Fig. 15. Distribution of heating in the troposphere (°C day^{-1}) due to the absorption of insolation by water vapor, *clear skies.*

where $\bar{q}$ is the average specific humidity in the layer, and Z is the average value of $\cos^{0.7}\zeta$ integrated over the solar day.

If the vertical distribution of absorption is known, however, the temperature changes in finite layers due to absorption of insolation can be computed with sufficient accuracy by the method used to determine infrared cooling. Thus,

$$\Delta T = 5.9 \times 10^3 \, \Delta a/\Delta p, \tag{34}$$

where ΔT is the temperature change in °C day^{-1} due to the absorption in a layer of Δp mb thick, if compressional effects are neglected.

5.51. *Clear Skies*

Temperature changes resulting from the absorption of insolation in the troposphere have been investigated by Möller (1935), Tanck (1940) and others. By the use of Mügge and Möller's adaptation of Fowle's absorption distribution (discussed above), Möller determined the average vertical distribution of heating for June over Lindenberg (52° N). His results show a minimum of heating at 1 km of about 0.2°C day^{-1} increasing to a maximum of about 0.5°C day^{-1} at 6 km and then decreasing above 6 km Tanck, using Eq. (33), calculated the effect of the temperature and relative humidity distribution on heating in the atmosphere by water vapor absorption. Two different temperature curves were assumed, and for each of these he assumed three relative humidity distributions corresponding to conditions in the center of an anticyclone and directly east and west of a cyclone. In all cases where the relative humidity increased or remained constant, the maximum warming (about 0.7°C day^{-1}) occurred at the top of the layer of constant or increasing relative humidity. He also computed the heating distribution up to 6 km for data representing a three-year average (1936–1938) of temperature and moisture over Hamburg (53° N). The average curves for March show a rate of heating of about 0.6°C day^{-1} from the surface to about 3 km decreasing to about 0.4°C day^{-1} at 6 km.

In the present calculations the distribution of heating in the troposphere by the absorption of water vapor was determined for each 10° latitude belt. The temperature changes were computed by means of Eq. (34) and Table 10 and therefore include the effect of pressure on the distribution of absorption. The variation of heating with latitude and with height is shown in Fig. 15 for clear skies.

The results generally confirm the order of magnitude found by previous investigators. Although small when compared to the rate of infrared cooling, the values of the computed heating are by no means negligible, amounting in some cases to about 50 percent of the temperature changes due to infrared cooling. The largest heating values (about 0.7°C day^{-1}) are found in the lower troposphere (0 to 5 km) in the region 0° to 20° N. Despite the longer path lengths of the solar beam, the heating decreases northward (0.1°C day^{-1} at 60° to 70° N) because of the rapid decrease of total precipitable water with latitude. In the upper troposphere (at 10 km) the heating is about 0.4°C day^{-1} at 0° to 10° N decreasing to about 0.1°C day^{-1} at 60° to 70° N. This results from the fact that even at 10 km our physical model shows more precipitable water in the equatorial than in polar regions. It should be pointed out that the heating values in the upper troposphere are, at best, merely estimates of the magnitude of the actual temperature changes.

5.52. Reflection, Transmission and Absorption by Clouds

The distribution of heating discussed in the preceding section is considerably altered by the presence of clouds in the atmosphere. This results from the fact that absorption of insolation by cloud particles in the near infrared is somewhat larger than absorption by water vapor and, more important, the large scattering by water droplets greatly reduces the transmitted insolation that could be absorbed by water vapor below the cloud.

The generally accepted value of the average reflectivity of clouds has heretofore been that given by Aldrich (1919). Aldrich's value of the cloud albedo (78 percent) was based on the average of about 100 observations of the incident and reflected radiation from the tops of stratus and fog in the valley adjacent to Mt. Wilson. No apparent relationship was found between cloud thickness and reflectivity.

Neiburger (1949) has recently presented observations of the absorption and reflection of clouds under conditions similar to those studied by Aldrich. Almost simultaneous pyrheliometric measurements of total upward and downward radiation were made above and below stratus clouds, on about 50 days during the summer of 1945. He found, contrary to Aldrich's conclusions, that the reflectivity changed markedly with changes in cloud depth, being very small when the cloud is thin and increasing to about 80 percent when the cloud depth is about 2000 ft. The average distribution of drop size in the clouds studied shows a mode at a radius of about 7×10^{-4} cm. The liquid water content was found to increase from the base to the top of the clouds with an average water density of about 0.3 gm m^{-3}.

The effect of the size and density of cloud particles and the thickness of the cloud on the reflection, transmission and absorption of solar radiation by clouds has been studied theoretically by Hewson (1943). Hewson showed that for a cloud with droplet radius of 5×10^{-4} cm and liquid water density 1.0 gm m^{-3}, the reflectivity increases with cloud depth from about 38 percent for a depth of 20 meters to about 93 percent for a depth of 4000 meters. The absorptivity by the cloud, under the same conditions of drop size and density, increases from 0.6 percent at 20 meters to about 6.5 percent for a depth of 4000 meters. It was also shown that for a cloud 200 meters thick, 80 percent of the absorption takes place in the top 100 meters of the cloud.

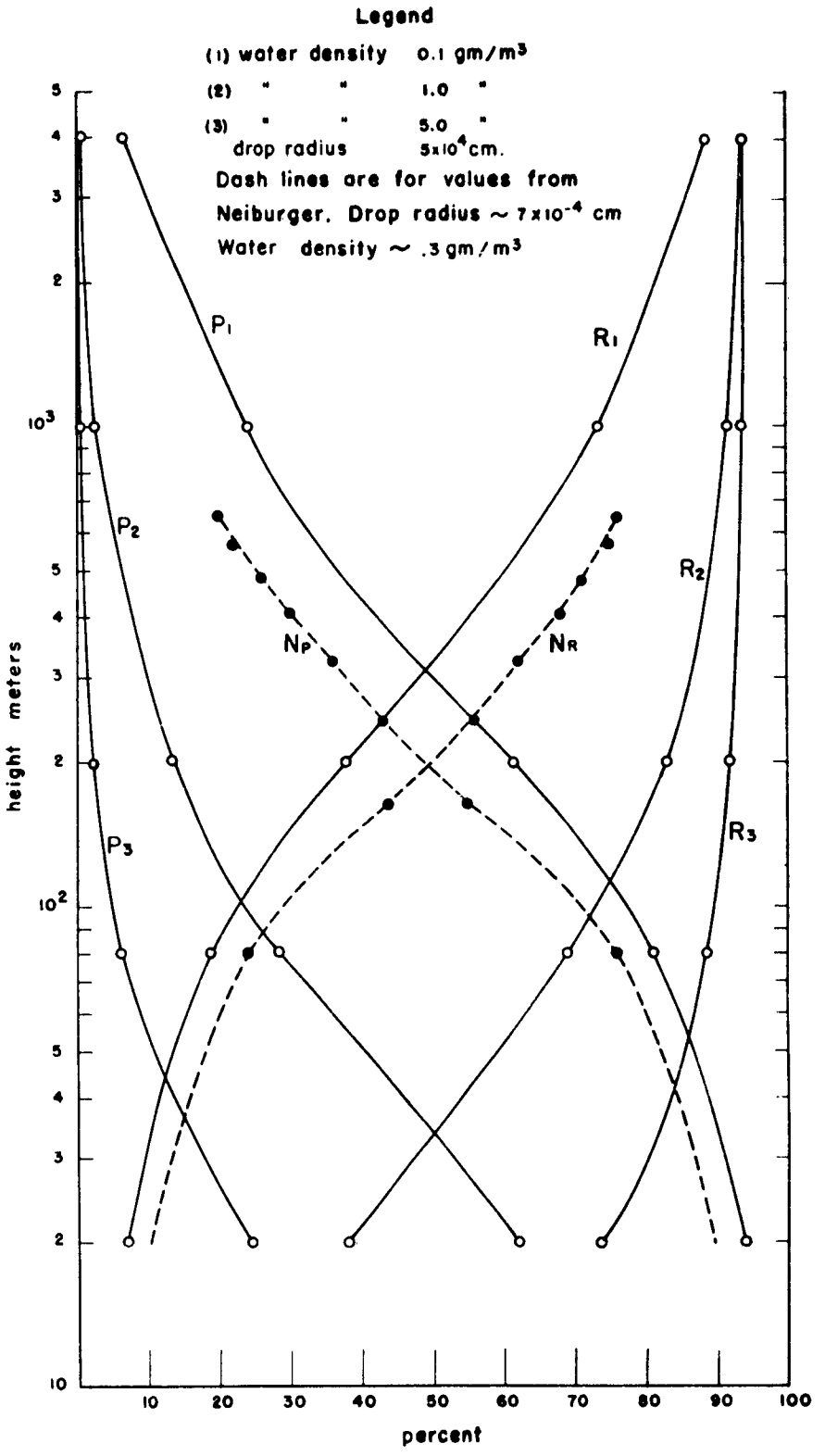

Fig. 16. Relationship between reflectivity (R), transmissivity (P) and cloud depth (after Hewson).

The results published by Hewson indicate that there is practically no variation of reflection, transmission or absorption with solar zenith distance. This is generally confirmed by the data published by Haurwitz (1948) of the ratio between insolation received on a horizontal surface at Blue Hill Observatory for overcast skies of various cloud types to that received for clear skies. The data indicates that the transmission decreases from about 80 percent for high clouds (Ci to Cs) to about 20 percent for fog and Ns. There is very little change in transmission shown for a change in zenith angle from 0° to 75°. Since all of the cloud observations were made at the ground, there were no reports of cloud thickness to relate the change of transmission to cloud depths.

From the results discussed above, it is evident that Aldrich's value for the albedo of clouds is probably correct for typical stratus about 2000 ft. thick, but does not represent the average reflectivity of clouds independent of cloud structure and cloud depth. The distribution of percentual reflection and transmission of incident insolation as a function of cloud depth, as determined by Hewson, is shown in Fig. 16 for a drop radius of 5×10^{-4} cm. Three sets of curves are drawn corresponding to liquid water densities of 0.1, 1.0 and 5.0 gm m^{-3}. The absorption distribution for a constant drop size and cloud density is determined from the curves of reflection and transmission since the percentual absorption is

$$A = 1 - (R + P), \tag{35}$$

where R is the reflectivity and P is the transmissivity. A set of curves based on the data taken from Neiburger's paper is included to show the consistency between the observed and theoretically derived data.

It is seen from the curves in Fig. 16, that for constant drop size and cloud density, the absorption and reflection increase while the transmission decreases with increasing cloud depth.

There is, of course, a wide variation in drop size and cloud density not only from cloud to cloud, but also within the same cloud. For the present investigation it is sufficient to consider average cloud structures by cloud type and to assume approximate homogeneity within each cloud group. Hewson (1943) quotes Bricard's measured values of drop radii for various types of clouds. Similar values are given by aufm Kampe (1950) based on the airplane measurements of Diem. Aufm Kampe also gives values of the liquid water content computed for various types of clouds.

Table 11 presents the values of average drop radius and liquid water content for each of the cloud groups used in the present study.

Table 11. Average drop radius and liquid water density by cloud groups.

Cloud group	Radius (10^{-4} cm)	Density gm m^{-3}
Cirrus	1	0.1
Cumulonimbus	10	2 5
Altostratus-altocumulus	5	0.2
Cumulus	5	0.5
Stratocumulus-fractocumulus	5	0.3
Nimbostratus	10	0.5

The cloud depths, in general, vary with latitude. The thicknesses assumed in the following discussion for each cloud group, are based on the values of the tops and bases given for each latitude belt in Section 3 of this report. For the As and Stcu cloud depths, a constant thickness of 200 meters was used for all latitudes.

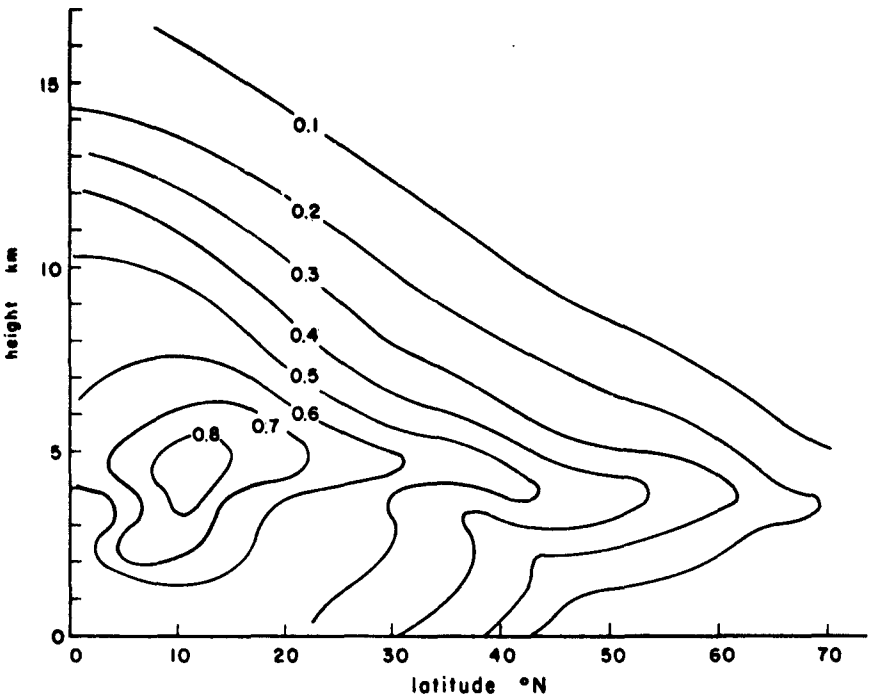

Fig. 17. Distribution of heating in the troposphere (°C day^{-1}) due to the absorption of insolation by water vapor and clouds, *average cloudiness.*

5.53. *Absorption and Heating for Average Cloudiness*

It has been pointed out previously that the heating in the atmosphere, resulting from absorption of insolation, is affected by the presence of clouds because of the absorption of the cloud layer and the reduced transmission of insolation resulting from the high reflectivity of the clouds.

The inclusion of absorption by clouds in the calculations of heating in the troposphere introduces a number of factors which increase the complexity of the computations out of proportion to the increased accuracy of the heating values. The following assumptions were therefore made in order to simplify the computations and still maintain a reasonable picture of the role played by clouds in the heating of the atmosphere.

1. There is no overlap of clouds along the solar beam.
2. The absorption by the cloud layer contributes to the total absorption in the kilometer interval of which the cloud top is a part.
3. Absorption at the sides of clouds is small and can therefore be omitted in the calculation.
4. Absorption by water vapor of the insolation reflected by clouds and the earth's surface is small and can be neglected.

The percentage absorption by clouds for each latitude belt was computed for the thickness of each cloud group from the appropriate curves in Fig. 16. The energy absorbed by the cloud layer in cal cm^{-2} min^{-1} was then found by considering the insolation incident to the cloud and the percentage of sky cover for each cloud group. To this was added the energy absorbed by water vapor for each kilometer interval. The latter was found by reducing the absorption by water vapor determined in the case of clear skies by a factor based on the reduced transmission of insolation resulting from the presence of clouds.

The distribution of heating in the troposphere considering average cloudiness is calculated from Eq. (34) where Δp represents the pressure difference for each kilometer interval. This distribution (Fig. 17) shows that the maximum heating is no longer found near the surface but at the level of the middle clouds. In the equatorial regions the largest heating values are at about 5 km (0.8°C day^{-1}) and in the polar regions the largest heating values are at about 3.5 km (0.25°C day^{-1}). It is interesting to note that although the local heating at the predominant cloud levels has been increased as a result of the absorption by clouds, the heating below the clouds has been reduced. This is due to the fact that the clouds transmit, on the average, only about 60 to 70 percent of the incident insolation. The reduced transmission results in a noticeable reduction in the absorption by water vapor below the cloud layers. The heating of the upper troposphere is not affected by cloudiness. This is borne out by a comparison of Figs. 15 and 17. Just below the tropopause the temperature changes shown on both charts are very small, amounting to about 0.1 to 0.2°C day^{-1}.

6. THE DISTRIBUTION OF *NET* RADIATIONAL TEMPERATURE CHANGE IN THE TROPOSPHERE

The net radiational temperature change in the troposphere is the difference between the infrared cooling and the heating due to absorption of insolation. For both clear and average cloudy skies the entire troposphere loses heat through radiation. This is because of the nature of the vertical distribution of water vapor in the atmosphere, and the fact that water vapor and liquid water absorb and emit radiational energy much more effectively in the infrared and near infrared than in the visible part of the spectrum. For all latitudes, the heat loss is a maximum in the middle troposphere for both clear and cloudy skies.

6.1. CLEAR SKIES

The level of maximum *net* cooling in the case of clear skies varies from about 10 km near the equator to about 3 km at latitudes 60° to 70° N (Fig. 18). The value of this maximum cooling decreases from about 1.5°C day^{-1} near the equator to about 0.8°C day^{-1} in the more northerly regions. In the lowest 2 km, the rate of cooling at most latitudes is quite constant at about 0.7°C day^{-1}. The lower layers in the subtropical region cool at a slightly higher rate (about 0.9°C day^{-1}) because the rapid decrease of water vapor with height permits more infrared radiation to be lost to space. Aloft, near the tropopause, the net cooling varies from about 1.0°C day^{-1} (0.10° N) to about 0.5°C day^{-1} (60° to 70° N). Thus, contrary to the results of Möller (1935) but in support of those of Albrecht (1950) it is found that, even in the case of clear skies, radiational processes lead to the development of thermal instability in the lower layers of the troposphere.

6.2. AVERAGE CLOUDINESS

The pattern of net cooling is somewhat modified if the distribution of average cloudiness is considered (Fig. 19). The level of maximum cooling is lowered at all latitudes except near the equator. Here, above about 3 km, the air cools at a fairly constant rate of about 1.2° to 1.4°C day^{-1}. The approximate level of

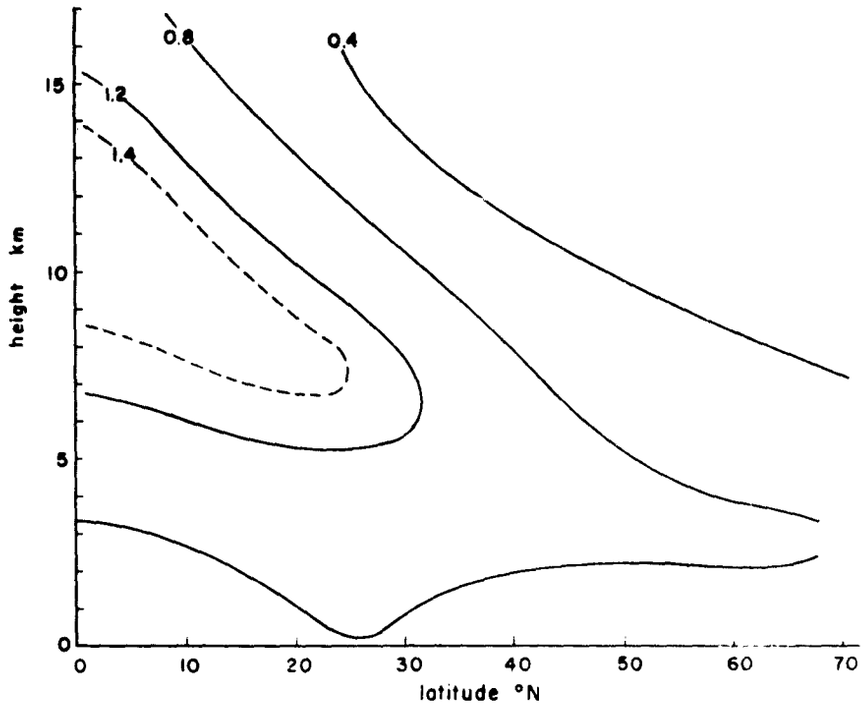

Fig. 18. Net radiational cooling in the troposphere (°C day^{-1}), *clear skies*.

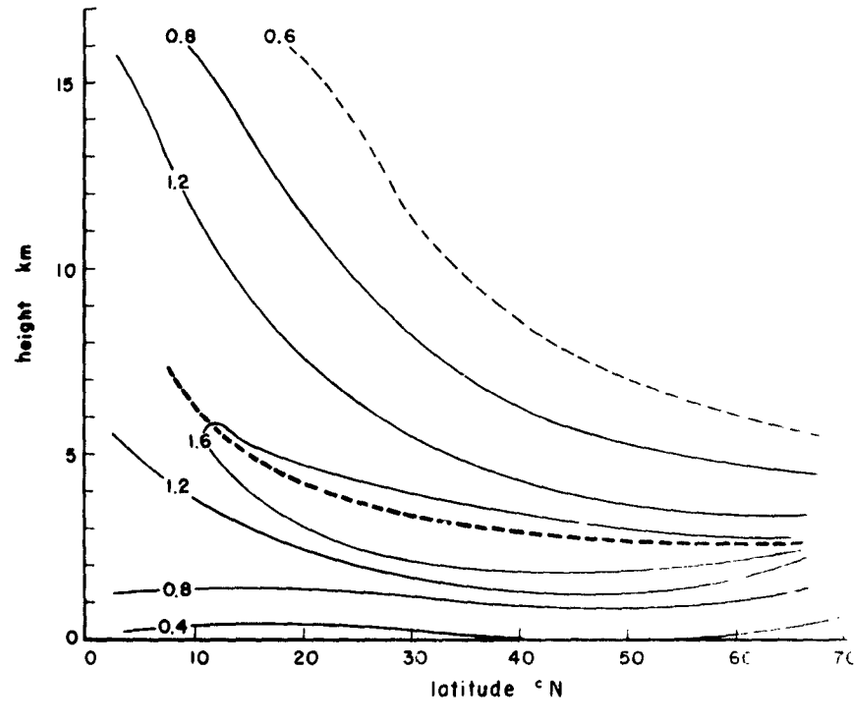

Fig. 19. Net radiational cooling in the troposphere (°C day^{-1}), *average cloudiness*.

maximum cooling, which is indicated by the heavy dashed line in Fig. 19, varies from about 5 km at 10° to 20° N to about 2.5 km at 60° to 70° N. The rate of net cooling at this level is about 1.8°C day^{-1}.

The most striking and climatologically important difference between the net cooling distribution for clear skies and that for a troposphere containing average cloudiness is that the cooling at the middle cloud level has almost everywhere been increased — in the polar regions this cooling has actually been doubled as a result of the presence of clouds — and the cooling in the lowest kilometer has been markedly decreased. This produces a gradient of temperature change which is about two or three times larger for average cloudiness than for clear skies. The marked effect of cloudiness, therefore, is to intensify the development of radiational instability in the layers below the level of the middle clouds.

Above the level of maximum cooling, the gradient of temperature change is of opposite sign and weaker than the gradient below this level. This results in a stabilization of the upper levels and is independent of cloudiness in the troposphere.

6.3. THE AVERAGE RADIATIONAL COOLING OF THE TROPOSPHERE

The average radiational temperature change in the troposphere can be computed by considering the radiation flux divergence between the surface and the tropopause for each latitude belt. The distribution with latitude of this average radiational temperature change is shown in Table 12. Columns a and b represent the cooling due to infrared radiation and the heating due to absorption of insolation, respectively. A comparison of values in Table 12 for clear and cloudy skies shows that the average infrared cooling is not affected by cloudiness, except at higher latitudes where the infrared cooling has been increased slightly as a result of the clouds being concentrated at levels below 3 km. The heating due to absorption of insolation is not changed at all as a result of cloudiness. This results from the fact that the transmission of insolation is decreased, although there is increased absorption at the cloud levels; thus the absorption below these cloud levels is diminished. The net result is an average cooling, approximately constant with latitude, of about 1°C day^{-1}.*

During the month of March the average temperature in the troposphere is rising, albeit slowly. The energy required to raise the temperature by the observed amount is very small when compared to the energy lost by the atmosphere through radiation (Panofsky (1950)). Compensating processes must be present, therefore, to balance the radiational heat loss. These processes are sensible heat transfer through eddy conduction from the earth's surface and the release of latent heat by condensation.

In a stable atmosphere, the vertical transport of heat due to turbulence is small, and is directed downward (e.g., Haurwitz (1941), Robinson (1951)). Surface heating during the daytime, however, develops instability in the lower layers which aids the turbulent exchange of heat. Since the air is then unstable, the transport of heat will be upward to the top of the convective layer. Thus the vertical transport of sensible heat is aided when that transport is directed upward and suppressed when that transport is directed downward.

The source of atmosphere water vapor is at the earth's surface (the oceans). The vertical transport of latent heat is therefore always directed upward and this heat is realized by the atmosphere through condensation.

---

* It is interesting to note that this value of the heat loss by radiation in the troposphere is the same as the value computed by Gold about 40 years ago. (See the discussion on Radiation in the *Centenary Proceedings of the Royal Meteorological Society*, 1950.)

Table 12. The distribution of average radiational temperature change in the troposphere during March (°C day^{-1}).

	Clear Skies			Average Cloudiness		
ϕ° N	a	b	Net	a	b	Net
0°–10°	−1.6	+0.6	−1.0	−1.6	+0.6	−1.0
10°–20°	−1.6	+0.5	−1.1	−1.55	+0.5	−1.05
20°–30°	−1.45	+0.45	−1.0	−1.4	+0.4	−1.0
30°–40°	−1.2	+0.35	−0.85	−1.2	+0.35	−0.85
40°–50°	−1.1	+0.3	−0.8	−1.2	+0.3	−0.9
50°–60°	−0.9	+0.2	−0.7	−1.1	+0.2	−0.9
60°–70°	−0.65	+0.1	−0.55	−0.9	+0.1	−0.8

It is of some interest to compare estimates of magnitude of the energy involved for the heat sources and sinks for the atmosphere. The net radiational flux divergence corresponding to average cloudy skies during March for a column of unit cross section in the troposphere varies from 238 cal cm^{-2} day^{-1} at 0° to 10° N (depth 16 km) to 153 cal cm^{-2} day^{-1} at 60° to 70° N (depth 10 km). If this flux divergence is weighted by the relative area of each latitude belt, the average radiational heat loss during March for the entire troposphere (0° to 70° N) is 204 cal cm^{-2} day^{-1}.

The quantity of heat released to the atmosphere by condensation can be estimated from existing published data. If it is assumed that there is no change in average cloudiness amount through the month of March, the total quantity of water vapor which is condensed in the atmosphere falls to the ground as precipitation. Then the observed distribution of precipitation with latitude is a measure of the heat released by condensation, assuming that there is no divergence of the horizontal flux of liquid water across each latitude belt.

The zonal distribution of annual precipitation is given by Haurwitz and Austin (1944) after the data of Meinardus. For the region 0° to 70° N, the annual amount of precipitation is given as about 105 cm, or about 8.8 cm for March if that month is regarded as average with respect to precipitation. Haurwitz and Austin point out that the amount of precipitation taken from Meinardus' data is probably a little too high, since the precipitation falling over the ocean areas has been overestimated. Jacobs (1951) gives values of the zonal distribution of precipitation over the oceans for each season. His values indicate that a more correct amount of the precipitation falling in the region 0° to 70° N during March is about 7.5 cm. This corresponds to an energy release to the atmosphere of about 145 cal cm^{-2} day^{-1}, if all of the condensation occurs at a temperature of −10°C. Thus, heat of condensation offsets about 70 percent of the radiative heat loss.

There are very few reliable data on the average eddy flux of sensible heat from the ground to the atmosphere. From the values calculated for the radiational energy loss and that estimated for the latent heat gained by the atmosphere, it is seen that the conduction of heat to the atmosphere should be of the order of about 60 cal cm^{-2} day^{-1}. This would then represent the remaining 30 percent of the energy necessary to balance the energy lost through radiation.

6.4. CONCLUSIONS

The results stated in the preceding section indicate clearly that the troposphere constitutes an energy source insofar as its radiative properties are concerned. Although the net radiative heat loss is fairly uniform

from latitude to latitude, it is found that at all latitudes the largest radiative cooling is in the middle troposphere. This is because of the major importance of water vapor in atmospheric radiative heat transfer and the characteristic distributions of water vapor with height in the lower atmosphere.

The presence of clouds does not qualitatively alter the cooling distribution but more sharply defines the layer of maximum cooling and increases the heat loss in this layer. In this way cloudiness contributes to the development of thermal instability below about 3 to 5 km and thus aids in the transport of heat upward through eddy conduction of sensible heat and, more important, through eddy transfer of latent heat.

It was stated at the beginning of this paper that the primary function of the general circulation is to maintain an overall heat energy balance of the atmosphere. In the equatorial latitudes the energy of sensible and latent heat transported to the atmosphere is larger than that lost by the atmosphere through radiative processes. Indeed if one considers the balance between total incoming and total outgoing radiative currents at the top of the atmosphere, there is a net radiative excess for all latitude belts south of about 40° N (Baur and Philipps (1935), London (1951)).

In the polar regions, where the vertical transport of both sensible and latent heat is smaller than the radiative heat loss, it is found that there is a large radiation deficit between the total upward and total downward radiative currents at the top of the atmosphere. Thus the mechanism which describes the maintenance of an equilibrium heat budget for the troposphere must account for the predominantly vertical transport of heat in the equatorial and subtropical regions and horizontal (northward) transport in mid and polar latitudes.

The atmospheric circulation patterns which would promote such a redistribution of heat energy are different in equatorial than in midlatitude regions. In the equatorial and subtropical regions, the heat transport presumably takes place through the existence of large semipermanent meridional cells as first described by Hadley (1735). In midlatitudes, however, the poleward transport of heat energy is probably accomplished through the large-scale eddies which are associated with the major cyclones and anticyclones in the atmosphere (Jeffreys (1926)). Any proposed energy budget for the atmosphere should at least be qualitatively consistent with these circulation patterns.

7. REFERENCES

Abbot, C. G. (1942), *Ann. Astrophys. Obs. Smith. Instn.* 6, 207.

Abbot, C. G., F. E. Fowle and L. B. Aldrich (1923), "The Distribution of Energy in the Spectra of the Sun and Stars," *Smith. Misc. Coll.* 74, 30.

Adel, A. (1947), "Absorption Line-Width in the Rotation Spectrum of Atmospheric Water Vapor," *J. Opt. Soc. Amer.* 37, 516.

Albrecht, F. (1950), Untersuchungen über den Wärmehaushalt der Erdatmosphäre und seine thermodynamische Bedeutung. *Berichte des Deutschen Wetterdienstes in der U. S. Zone*, no. 17, 70.

Aldrich, L. B. (1919), "The Reflecting Power of Clouds," *Smith. Misc. Coll.* 69, 9.

Atlas of Climatic Charts of the Oceans (1938), United States Government Printing Office, Washington, D. C.; 130 pp.

aufm Kampe, H. J. (1950), "Visibility and Liquid Water Content in Clouds and in the Free Atmosphere," *J. Meteor.* 7, 54–57.

Barrett, E. W., L. R. Herndon, Jr. and H. J. Carter (1949), "A Preliminary Note on the Measurement of Water Vapor Content in the Middle Stratosphere," *J. Meteor.* 6, 367–368.

———(1950), "Some Measurements of the Distribution of Water Vapor in the Stratosphere," *Tellus* 2, 302–311.

Baum, W. A., F. S. Johnson, J. J. Oberly, C. C. Rockwood, C. V. Strain and R. Tousey (1946), "Solar Ultraviolet Spectrum to 88 km," *Phys. Rev.* 70, 781–782.

Baur, F. and H. Philipps (1935), "Der Wärmehaushalt der Lufthülle der Nordhalbkugel in Januar und Juli zur Zeit der Aquinoktien und Solstitien," *Ger. Beitr. z. Geo.* 45, 82–132.

Best, N., R. Havens and H. Lagow (1947), "Pressure and Temperature of the Atmosphere to 120 km," *Phys. Rev.* 71, 915–916.

Bjerknes, V., J. Bjerknes, H. Solberg and T. Bergeron (1933), *Physikalische Hydrodynamik*, Julius Springer, Berlin; 799 pp.

Brasefield, C. J. (1950), "Winds and Temperatures in the Lower Stratosphere," *J. Meteor.* 7, 66–69.

Brewer, A. W. (1949), "Evidence for a World Circulation Provided by the Measurements of Helium and Water Vapor Distribution in the Stratosphere," *Quart. J. Roy. Meteor. Soc.* 75, 351–363.

Brewer, A. W., B. Cwilong and G. M. B. Dobson (1948), "Measurement of Absolute Humidity in Extremely Dry Air," *Proc. Phys. Soc.* 60, 52–70.

REFERENCES (Continued)

Brooks, C. E. P. (1927), "Mean Cloudiness Over the Earth," *Mem. Roy. Meteor. Soc.* 1, 127–138.

Brooks, D. L. (1948), "Measurements of Atmospheric Radiation Applied to the Heat Transfer by Infra-red Radiation in the Free Atmosphere," Ph.D. Thesis, Mass. Inst. Tech., Cambridge, Mass.

——— (1950), "A Tabular Method for the Computation of Temperature Change by Infra-red Radiation in the Free Atmosphere," *J. Meteor.* 7, 313–321.

Brooks, F. A. (1941), "Observations of Atmospheric Radiation," *Papers in Physical Oceanography and Meteorology*, Mass. Inst. Tech. and Woods Hole Ocean. Instn., 8, 1–23.

Bruinenberg, A. (1946), "Een numerieke method voor de bepaling van temperatuurs veranderingen door straling in de vrije atmosfeer," *K. Ned. Inst. Meteor. Inst. Verh.* Serie B, Deel 1, no. 1; 52 pp.

Brunt, D. (1939), *Physical and Dynamical Meteorology*, 2nd ed., Cambridge Univ. Press, London; 428 pp.

———(1940), "Radiation in the Atmosphere," *Quart. J. Roy. Meteor. Soc.* (Suppl.) 66, 34–40.

Brunt, D. and A. Kapur (1938), "The Amount of Water Vapor in the Stratosphere and Upper Troposphere," *Quart. J. Roy. Meteor. Soc.* 64, 510–515.

Callendar, G. S. (1940), "Variations in the Amount of Carbon Dioxide in Different Air Currents," *Quart. J. Roy. Meteor. Soc.* 66, 395–400.

———(1941), "Infra-red Absorption by Carbon Dioxide With Special Reference to Atmospheric Radiation," *Quart. J. Roy. Meteor. Soc.* 67, 263–275.

Chapman, R. M. (1950), "The Absorption of Radiation in the Very Near Infra-red by Water Vapor," *Phys. Rev.* 77, 741.

Charney, J. (1945), *Handbook of Meteorology* (ed. by Berry, F. A., Jr., E. Bollay and N. R. Beers), McGraw-Hill, New York; pp. 284–311.

Chiplonkar, M. W. (1940), "The Distribution of Temperature in the Lower Stratosphere," *Proc. Ind. Acad. Sci.* 11, 39–51.

Colange, G. (1927), "Etude de l'absorption par l'ozone dans le spectre visible," *J. Phys. Radium* 6, 254–256.

Cowling, T. G. (1950 a), "Atmospheric Absorption of Heat Radiation by Water Vapor," *Phil. Mag.* 41, 109–123.

———(1950 b), "The Calculation of Radiative Temperature Changes," *Cent. Proc. Roy. Meteor. Soc.*, pp. 19–25.

REFERENCES (Continued)

Cox, E. F., J. V. Atanasoff, B. L. Snavely, D. W. Beecher and J. Brown (1949), "Upper Air Temperatures From Helgoland Big Bang," *J. Meteor.* 6, 300–311.

Craig, R. A. (1949), "Radiative Heating and Cooling of the Ozone Layer," *Special Report*, Harvard Univ., Cambridge, Mass.; 39 pp.

———(1950), "The Observations and Photochemistry of Atmospheric Ozone and Their Meteorological Significance," *Meteor. Mono.* 1, 50.

Deacon, E. L. (1950), "Heat Transfer in the Air Near the Ground," *Aust. J. Sci. Res. A* 3, 274–283.

Dennison, D. M. (1928), "The Shape and Intensities of Infra-red Absorption Lines," *Phys. Rev.* 31, 503–519.

Dobson, G. M. B. (1942), "Atmospheric Radiation and the Temperature of the Lower Stratosphere," *Quart. J. Roy. Meteor. Soc.* 68, 202–204.

Dobson, G. M. B., A. W. Brewer and B. M. Cwilong (1946), "Meteorology in the Lower Atmosphere," *Proc. Roy. Soc.* 185A, 144–175.

Durand, E. and R. Tousey (1947), NRL Rept. No. R 3120, *Upper Atmosphere Research*, no. 3.

Elsasser, W. M. (1938), "Mean Absorption and Equivalent Absorption Coefficient of a Band Spectrum," *Phys. Rev.* 54, 126–129.

———(1940 a), "Radiative Cooling in the Lower Atmosphere," *Mon. Wea. Rev.* 68, 185–188.

———(1940 b), "An Atmospheric Radiation Chart and Its Use," *Quart. J. Roy. Meteor. Soc.* (Suppl.) 66, 41–56.

———(1941), "A Heat Radiation Telescope and the Measurement of Infra-red Emission of the Atmosphere," *Mon. Wea. Rev.* 69, 1–5.

———(1942), "Heat Transfer by Infra-red Radiation in the Atmosphere," *Harvard Meteor. Studies*, Blue Hill Meteor. Obs. No. 6; 105 pp.

Flohn, H. (1947), "Die mittlers Höhenlage der Tropopause über der Nordhalbkugel," *Met. Rdsch.* 1 2, 26–29.

Fowle, F. E. (1915), "The Transparency of Aqueous Vapor," *Astrophys. J.* 42, 394–411.

———(1917), "Water Vapor Transparency to Low Temperature Radiation," *Smith. Misc. Coll.* 68, pp. 1–68.

Fritz, S. (1949), "The Albedo of the Planet Earth and of Clouds," *J. Meteor.* 6, 277–282.

REFERENCES (Continued)

Gluckauf, E. (1944 a), "Notes on Upper Air Hygrometry. I. Calculation of the Relative Humidity From Hair Hygrometer Readings During Balloon Ascents," *Quart. J. Roy. Meteor. Soc.* **70**, 293–301.

———(1944 b), "Carbon Dioxide Content of the Free Air," *Nature* **20**, 620–621.

———(1945), "Notes on Upper Air Hygrometry. II. On the Humidity in the Stratosphere," *Quart. J. Roy. Meteor. Soc.* **71**, 110–114.

Götz, F. W. P. (1949), "Der Stand des Ozonproblems," *Berichte des Deutschen Wetterdienstes in der U. S. Zone*, no. 11, 7–13.

Götz, F. W., A. R. Meetham and G. M. Dobson (1934), "The Vertical Distribution of Ozone in the Atmosphere," *Proc. Roy. Soc.* **145A**, 416–446.

Grimminger, G. (1947), "Analysis of Temperature, Pressure and Density of the Atmosphere Extending to Extreme Altitudes," *Project Rand*, Douglas Air Craft Co., Inc.; 97 pp.

Hadley, G. (1735), "Concerning the Cause of the General Trade-Winds," *Phil. Trans.* **39**, 58–63.

Hales, J. V. (1950), "An Atmospheric Radiation Flux Divergence Chart." Paper presented at meeting of A. M. S., Washington, D. C., 1-3 May 1950. (Personal communication.)

Hann, J.-R. Süring (1938), (ed. by R. Süring) *Lehrbuch der Meteorologie*, 5th ed., Willibald Keller, Leipzig; pp. 332–335.

Haurwitz, B. (1941), *Dynamic Meteorology*, McGraw-Hill, New York; 365 pp.

Haurwitz, B. (1948), "Insolation in Relation to Cloud Type," *J. Meteor.* **5**, 110–113.

Haurwitz, B. and J. M. Austin (1944), *Climatology*, McGraw-Hill, New York; pp. 89–95.

Hess, S. (1948), "Some New Mean Meridional Cross Sections Through the Atmosphere," *J. Meteor.* **5**, 283–300.

Hettner, G. (1918), "Ueber das ultrarote Absorptions spektrum des Wasserdampfes," *Ann. Physik*, **55**, 476–496.

Hewson, E. W. (1943), "The Reflection, Absorption and Transmission of Solar Radiation by Fog and Cloud," *Quart. J. Roy. Meteor. Soc.* **69**, 47–62.

Hoelper, O. (1937), "Über die Bestimmung der Atmosphärischen Trübung und des Wasserdampfgehalts aus Strahlungsmessungen," *Meteor. Zeits.* **54**, 458–460.

———(1943), "Über die Absorption des Wasserdampfes im Sonnenspektrum," *Meteor. Zeits.* **60**, 37–42.

REFERENCES (Continued)

Hoffer, T. E. (1951), "A Study of the Long Wave Radiation Balance in Certain Typical Air Masses," Atmospheric Radiation Research Project, Rept. 5, Meteorology Department, Univ. Utah.

Hulbert, E. O. (1947), "The Upper Atmosphere of the Earth," *J. Opt. Soc. Amer.* 37, 405–415.

Humphreys, W. J. (1940), *Physics of the Air*, McGraw-Hill, New York; 676 pp.

Jacobs, W. C. (1951), "The Energy Exchange Between Sea and Atmosphere and Some of Its Consequences," *Bull. Scripps Inst. Ocean.*, Univ. Calif., La Jolla, Calif.; 122 pp.

Jeffreys, H. (1926), "On the Dynamics of the Geostrophic Wind," *Quart. J. Roy. Meteor. Soc.* 52, 85–104.

Junge, C. (1937), "Zur Strahlungswerkung des Wasserdampfes in der Stratosphäre," *Meteor. Zeits.* 54, 161–164.

Kaplan, L. D. (1952 a), "On the Pressure Dependence of Radiative Heat Transfer in the Atmosphere," *J. Meteor.* 9, 1–12.

———(1952 b), "On the Calculation of Atmospheric Transmission Functions for the Infra-red," *J. Meteor.* 9, 139–144.

Karandikar, R. V. (1946), "Radiation Balance of the Lower Stratosphere — I," *Proc. Ind. Acad. Sci.* 23, 70–96.

Kimball, H. H. (1927), "Measurements of Solar Radiation Intensity and Determinations of Its Depletion by the Atmosphere," *Mon. Wea. Rev.* 55, 155–169.

———(1930), "Measurements of Solar Radiation Intensity and Determination of Its Depletion by the Atmosphere," *Mon. Wea. Rev.* 58, 43–52.

Ladenburg, R. and F. Reiche (1913), "Ueber Selective Absorption," *Ann. Physik.* 42, 181–209.

London, J. (1951), "A Study of the Atmospheric Heat Balance," Prog. Rept. 131.07, Contract No. AF 19(122)-165, Res. Div., Coll. Engrg., New York Univ.

Lönnquist, O. (1950), "A General Method and a Simplified Formula for Calculating Effective Radiation," *Ark. Geofysik*, Utgivet au kungl. Svensky Vetenskapsakademien, 1, 79–115.

Matossi, F., R. Mayer and E. Rauscher (1949), "On the Total Absorption in Spectra With Overlapping Lines," *Phys. Rev.* 76, 760–764.

Matossi, F. and E. Rauscher (1949), "Zur Druckabhängigkeit der Gesamtabsorption in ultraroten Bandenspektren," *Zeits. Phys.* 125, 418–422.

REFERENCES (Continued)

Möller, F. (1935), "Die Wärmequellen in der freien Atmosphäre," *Meteor. Zeits.* 52, 408–412.

———(1944), "Grundlagen eines Diagramms zur Berechnung langwelliger Strahlungsstrome," *Meteor. Zeits.* 61, 37–45.

Möller, F. and R. Mügge (1931), "Temperaturänderungen in der Atmosphäre infolge der langwelligen Strahlung des Wasserdampfes," *Meteor. Zeits.* 48, 475–476.

Mügge, R. and F. Möller (1932 a), "Über Abkühlungen in der freien Atmosphäre infolge der langwelligen Strahlung des Wasserdampfes," *Meteor. Zeits.* 49, 95–104.

———(1932 b), "Zur Berechnung von Strahlungsströmen und Temperaturänderungen in Atmosphären von beliebigem Aufbau," *Zeits. Geophys.* 8, 53–64.

Murgatroyd, R. J. and C. T. B. Clews (1949), "Winds at 100,000 ft Over Southeast England," *Geophys. Mem.* no. 82, Meteorological Office, London.

Neiburger, M. (1949), "Reflection, Absorption and Transmission of Insolation by Stratus Cloud," *J. Meteor.* 6, 98–104.

Newell, H. E. (1950), "A Review of Upper Atmosphere Research From Rockets," *Trans. Amer. Geophys. Un.*, v. 31, pp. 25–34.

Nielsen, H. H. (1941), "The Near Infra-red Spectrum of Water Vapor, Part I, Perpendicular Bands ν_2 and $2\nu_2$ (6.25 μ)," *Phys. Rev.* 59, 565–574.

Ny, T. Z. and S. P. Choong (1932), "L'absorption de la lumiere par l'ozone entre 3050 et 3400 A (regions des bandes des Huggins). *Comptes Rendus de l'Acad. Sci.*, v. 195, pp. 309–311.

———(1933), "L'absorption de la lumiere par l'ozone entre 3050 et 2150 A," *Comptes Rendus de l'Acad. Sci.* 196, 916–918.

Oder, F. C. E. (1948), "The Magnitude of Radiative Heating in the Lower Stratosphere," *J. Meteor.* 5, 65–67.

Paneth, F. A. (1939), "Composition of the Atmosphere," *Quart. J. Roy. Meteor. Soc.* 65, 304–310.

Panofsky, H. A. (1950), "The Mean Meridional Circulation of the Northern Hemisphere in March," *Res. Rept.*, Dept. Meteor. Coll. Engrg., New York Univ., New York; 95 pp.

Penndorf, R. (1946 a), "The Temperature of the Upper Atmosphere," *Bull. Amer. Meteor. Soc.* 27, 331–342.

———(1946 b), "The Constitution of the Stratosphere," *Bull. Amer. Meteor. Soc.* 27, 343–345.

———(1950), "Absorption of Solar Energy by Oxygen in the E-Layer," *J. Meteor.* 7, 243–244.

REFERENCES (Continued)

Pettit, E. (1932), "Measurements of Ultraviolet Solar Radiation," *Astrophys. J.* 75, 185–221.

———(1940), "Spectral Energy-Curve of the Sun in the Ultraviolet," *Astrophys. J.* 91, 159–185.

Preliminary Climatic Atlas of the World (1943), Special Series No. 1 (Rev.). *Military Climatology Project*, Inst. Meteor., Univ. Chicago.

Ratner, B. (1946), "Upper Air Average Values of Temperature, Pressure and Relative Humidity Over U. S. and Alaska," *U. S. Wea. Bur. Tech. Rept. No.* 6, U. S. Dept. Commerce, Washington, D. C.

Regener, V. H. (1950), "Investigation in the Physics of Atmospheric Ozone," *Rept. No. 9*, Univ. New Mexico.

Robinson, G. D. (1947), "Notes on the Measurement and Estimation of Atmospheric Radiation," *Quart. J. Roy. Meteor. Soc.* 73, 127–150.

———(1950), "Notes on the Measurement and Estimation of Atmospheric Radiation," *Quart. J. Roy. Meteor. Soc.* 76, 37–51.

——(1951), "The Vertical Convective Heat Flux in the Atmosphere — a Critical Essay," *Quart. J. Roy. Meteor. Soc.* 77, 61–73.

Rossby, C.-G. (1941), "The Scientific Basis of Modern Meteorology," *Climate and Man Yearbook of Agriculture*, U. S. Government Printing Office, Washington, D. C.; pp. 599–655.

Shands, A. L. (1949), "Mean Precipitable Water in the U. S.," *Wea. Bur. Tech. Paper No. 10*, U. S. Weather Bureau, Washington, D. C.

Shaw, Napier (1936), *Manual of Meteorology*, Vol. 2, "Comparative Meteorology," Cambridge Univ. Press, London, pp. 145–168.

Sheppard, P. A. (1947), "Radiation in the Stratosphere and Troposphere," *Science Progress* 35, 87–101.

Simpson, G. C. (1928), "Further Studies in Terrestrial Radiation," *Mem. Roy. Meteor. Soc.* 3, 1–26.

Strong, J. and G. N. Plass (1950), "Heat Transfer in a Gravitational Atmosphere," *Prog. Rept. ONR*, Johns Hopkins Univ., Baltimore, Md.; 21 pp.

Strong, J. and K. Watanabe (1940), "Pressure Effect on Infra-red Absorption," *Phys. Rev.* 47, 1049.

Summerfield, M. and J. Strong (1941 a), "An Ultra Spectrometer Technique for Infra-red Absorption Bands," *Phys. Rev.* 59, 217–218.

———(1941 b), "Dependence of Band Absorption on Pressure," *Phys. Rev.* 60, 162.

REFERENCES (Continued)

Süring, R. (1931), "Der jetzige Stand der Wolkenforschung," *Meteor. Zeits.* **48**, 481.

Szava-Kovats, J. (1938), "Verteilung der Luftfeuchtigkeit auf die Erde," *Ann. Hydrographie*, **66**, 373–378.

Tanck, H. J. (1940), "Die tägliche Erwärmung der Atmosphäre infolge der Absorption der direkten Sonnenstrahlung durch den atmosphärischen Wasserdampf," *Ann. Hydrographie*, **68**, 47–63.

Tönsberg, E. and K. L. Olsen (1944), "Investigations in Atmospheric Ozone at Tromso," *Geofys. Publ.* **13**, 39.

United States Weather Bureau (1941), *Airways Meteorological Atlas*, Washington, D. C.

———(1944), *Normal Weather Maps, Northern Hemisphere*, Washington, D. C.

Vassey, A. (1941), "Sur l'absorption atmospherique dans l'ultraviolet," *Ann. Physique* **16**, 145–203.

Wagner, A. (1931), "Klimatologie der freien Atmosphäre in Köppen-Geiger," *Handbuch der Klimatologie*, I, part F, p. 65.

Yamamoto, G. (1949), "Average Vertical Distribution of Water Vapor in the Atmosphere," *J. Meteor. Soc. Japan* **27**, 277–282.

———(1950), "On Nocturnal Radiation," *J. Meteor. Soc. Japan* **28**, 1–20

Yamamoto, G. and G. Onishi (1949 a), "Absorption Coefficient of Water Vapor in the Near Infra-red Region," *J. Meteor. Soc. Japan* **27**, 269–276.

——— (1949 b), "Absorption Coefficients of Water Vapor in the Far Infra-red Region," Science Reports of the Tohuku Univ. Faculty of Science, Tohuku Univ., Sendai, Japan.

——— (1951), "Absorption of Solar Radiation by Water Vapor in the Atmosphere," to be published.

No. 1. Isotropic and Non-Isotropic Turbulence in the Atmospheric Surface Layer, Heinz Lettau, Geophysical Research Directorate, December 1949.

No. 2. (Classified)

No. 3. Diffraction Effects in the Propagation of Compressional Waves in the Atmosphere, Norman A. Haskell, Geophysical Research Directorate, March 1950.

No. 4. Evaluation of Results of Joint Air Force - Weather Bureau Cloud Seeding Trials Conducted During Winter and Spring 1949, Charles E. Anderson, Geophysical Research Directorate, May 1950.

No. 5. Investigation of Stratosphere Winds and Temperatures From Acoustical Propagation Studies, Albert P. Crary, Geophysical Research Directorate, June 1950.

No. 6. Air-Coupled Flexural Waves in Floating Ice, F. Press, M. Ewing, A. P. Crary, S. Katz, J. Oliver, Geophysical Research Directorate, November 1950.

No. 7. Proceedings of the Conference on Ionospheric Research (June 1949), edited by Bradford B. Underhill and Ralph J. Donaldson, Jr., Geophysical Research Directorate, December 1950.

No. 8. Proceedings of the Colloquium on Mesospheric Physics, edited by N. C. Gerson, Geophysics Research Division, July 1951.

No. 9. The Dispersion of Surface Waves on Multi-Layered Media, Norman A. Haskell, Geophysics Research Division, August 1951.

No. 10. The Measurement of Stratospheric Density Distribution With the Searchlight Technique, L. Elterman, Geophysics Research Division, December 1951.

No. 11. Proceedings of the Conference on Ionospheric Physics (July 1950) Part A, edited by N. C. Gerson and Ralph J. Donaldson, Jr., Geophysics Research Division, April 1952.

No. 12. Proceedings of the Conference on Ionospheric Physics (July 1950) Part B, edited by Ludwig Katz and N. C. Gerson, Geophysics Research Division, April 1952.

No. 13. Proceedings of the Colloquium on Microwave Meteorology, Aerosols and Cloud Physics, edited by Ralph J. Donaldson, Jr., Geophysics Research Division, May 1952.

No. 14. Atmospheric Flow Patterns and Their Representation by Spherical-Surface Harmonics, B. Haurwitz and Richard A. Craig, Geophysics Research Division, July 1952.

No. 15. Back-Scattering of Electromagnetic Waves From Spheres and Spherical Shells, A. L. Aden, Geophysics Research Division, July 1952.

No. 16. Notes on the Theory of Large-Scale Disturbances in Atmospheric Flow With Applications to Numerical Weather Prediction, Philip Duncan Thompson, Major, U. S. Air Force, Geophysics Research Division, July 1952.

No. 17. The Observed Mean Field of Motion of the Atmosphere, Yale Mintz and Gordon Dean, Geophysics Research Directorate, August 1952.